CrossMark

ORIGINAL PAPER

Dynamical analysis and FPGA implementation of a chaotic oscillator with fractional-order memristor components

Karthikeyan Rajagopal · **Anitha Karthikeyan** ·
Ashokkumar Srinivasan

Abstract Memristor-based chaotic and hyperchaotic systems are of great interest in the recent years, and addition of meminductor and memcapacitors to the family has widened the applications. In this paper, we propose a new chaotic system with fractional-order memristor and memcapacitor components. Nonlinear chaotic properties of the proposed system are investigated with equilibrium points, eigenvalues, Lyapunov exponents, bifurcation and bicoherence plots. We show that a small model disturbance can make the system to show self-excited and hidden attractors. We use the Adomian Decomposition method for implementing the proposed system in Field Programmable Gate Arrays.

1 Introduction

The fourth circuit element popularly known as memristors was first postulated by Chua [1]. Until 2008 when researchers of HP laboratories fabricated a solid-state implementation of memristor, none was known

K. Rajagopal (✉) · A. Karthikeyan
Center for Nonlinear Dynamics, Department of Electrical
and Communication Engineering, The PNG University of
Technology, Lae, Papua New Guinea
e-mail: rkarthiekeyan@gmail.com

K. Rajagopal · A. Karthikeyan · A. Srinivasan
Center for Nonlinear Dynamics, Defence University, Bishoftu,
Ethiopia

much about memristor realization [2]. Since then, many other memristor models have been introduced [5,6,34]. Memristors are considered to be highly nonlinear with nonvolatile characteristics and can be implemented with nanoscale technologies [5,6,34]. To design memristor oscillators, a new kind of nonlinear circuits with oscillatory memories and periodically forced flux-controlled memductance models are investigated [7,8].

Memristor-based chaotic oscillators are widely investigated in the last one decade. Circuits with two HP memristors in antiparallel are demonstrated showing a variety of chaotic attractors for different values of components [9]. A current feedback op-amp-based memristor oscillators are analyzed, and simulation results are investigated [10]. A simple autonomous memristor-based oscillator with external sinusoidal excitation is used to generate chaotic oscillations. A discrete model for this HP memristor is derived and implemented using DSP chips [11] implementing memristor. Recently a new hyper chaotic system with two memristors is investigated and its application to image encryption is analyzed. The correlation and ant attack capability between adjacent pixels are investigated [12].

Practical implementation of memristor-based chaotic circuits with off-the-shelf components is desired for real-time applications [13]. Memristor-based chaotic circuit for pseudo-random number generation is analyzed with applications to cryptography [14]. Memristor-based chaotic circuits for text and image

cryptography are investigated, and the correlation analysis shows the effectiveness of the proposed cryptographic scheme over other encryption algorithms [15]. Memcapacitor-based chaotic circuits with a HP memristor are proposed, and the analysis of the proposed oscillator is implemented in DSP for further applications [16].

Recently many researchers have discussed about fractional-order calculus and its applications [19–21]. Fractional-order nonlinear systems with different control approaches are investigated [22–24]. Fractional-order memristor-based no equilibrium chaotic and hyperchaotic systems are proposed [17,18,40,41]. A novel fractional-order no equilibrium chaotic system is investigated in [25], and a fractional-order hyperchaotic system without equilibrium points is investigated in [26]. Memristor-based fractional-order system with a capacitor and an inductor is discussed [27]. Numerical analysis and methods for simulating fractional-order nonlinear system are proposed in [28], and matlab solutions for fractional-order chaotic systems are discussed in [29]. Fractional-order multiscroll systems are also investigated in the recent years [87,88]

Implementation of chaotic and hyperchaotic system using field-programmable gate arrays (FPGA) is widely investigated [31–33]. Chaotic random number generators are implemented in FPGA for applications in image cryptography [34]. FPGA-implemented Duffing oscillator-based signal detectors are proposed [35]. Digital implementations of chaotic multiscroll attractors are extensively investigated [31,36]. Memristor-based chaotic system and its FPGA circuits are discussed with their qualitative analysis [37]. A FPGA implementation of fractional-order chaotic system using approximation method is investigated recently for the first time [17,18,40,41].

Analysis of dynamical systems starts from finding the fixed points. Physically equilibrium points are known as fixed points where the system is definitely stable. Hence, the characteristics of equilibrium lead to identify the complexity of the system. Initially chaotic systems without equilibria were commonly rejected as "incomplete" or "mis-formulated" [72]. Certain systems with hidden attractor show multistability for a range of parameter, and controlling such multistability feature is achieved with coupling of nonlinear systems with a linear system as discussed in [90] and using linear augmentation in [91]. The numerical difficulties associated with the location of complex nonlinear

states whose basin of attraction does not overlap with each other lead to the term "hidden attractor" [73]. The challenges in finding the hidden attractors make the no equilibrium systems more fascinate [74]. No equilibrium systems are more suitable and work effectively to design random number generators [75]. Hidden attractors affect the system performance vigorously and lead to system failure, so study of these systems becomes mandatory, especially in electromechanical systems [76]. Leonov and Kuznetsov studied [78–83] and developed [77–80] analytical and numerical methods to investigate the chaotic and hyperchaotic hidden attractors. A list of 17 structurally different 3D systems that display quadratic chaotic flows without equilibria [84] and new ways of analyzing stability of fractional-order systems are presented in [89]. Recently many new chaotic systems which can be controlled with a offset or boosting parameter are discussed [93–97].

2 Problem formulation

Many scientific and engineering fields such as physics, bioengineering, viscoelasticity theory, fractal dynamics, fractional control, signal and image processing presently, digital and analog communication, cryptography and secure communications use fractional calculus [61–64]. The application of fractional calculus to analyzing the memelements is an emerging discipline of study in which few studies have been performed [9–16,49,65–67]. In the engineering fields such as signal analysis and processing, circuits and systems, there are many issues on nonlinear, non-causal, non-Gaussian, non-stationary, non-minimum phase, non-white additive noise, non-integer-dimensional and non-integer-order characteristics needed to be analyzed and processed [67]. The classical integer-order signal processing filters and circuit models cannot deal with the aforementioned non-problems efficiently. Hence, fractional calculus has gained importance in signal and image processing, circuits and systems, etc.

As per Chua's axiomatic element system [1–6,64], there should be a novel corresponding capacitive circuit element and inductive circuit element to the capacitive fractor and inductive fractor, respectively. Therefore, it is important to investigate a challenging theoretical problem to determine memfractor elements and their positions in the Chua's axiomatic element. Also it is worth to investigate the applications of such memfrac-

tor elements. Motivated by these, we investigate the fractional order models of memristor and memcapacitor and use the memfractor elements to propose a novel chaotic oscillator.

Several memcapacitor models, including piecewise linear, quadric and cubic function models, memristor-based memcapacitor models, are discussed in several studies [50–53]. Some special phenomena such as hidden attractors, coexistence attractors and extreme multistability were found in memcapacitor-based chaotic oscillators [54–56]. Recently many researchers have worked on the fractional-order memristor (fracmemristor) models [65–67,69]. The ohmic relationship of a memristor is given by

$$R_{\text{in}} = lR_{\text{on}} + (1 - l)R_{\text{off}} \tag{1}$$

where l is the ratio of length of the doped region of memristor to the total length of the memristor, R_{on} is the minimum resistance and R_{off} maximum resistance of the memristor. The rate of change of l is given as,

$$\frac{\mathrm{d}l}{\mathrm{d}t} = \pm\lambda i(t)g(l) \tag{2}$$

where $\lambda = \frac{\mu_m R_{on}}{D^2}$ with μ_m denoting the dopant mobility, D is the length of memristor, and $g(l)$ is dopant drift given by $f(l) = 1 - (2l - 1)^{2p}$. The fractional memristor model is given by the relation

$$\frac{\mathrm{d}^q x}{\mathrm{d}t^q} = \pm\lambda i(t)g(l) \tag{3}$$

Solving (3) with (1), the input resistance of the memristor is derived as,

$$\frac{\mathrm{d}^q R_{\text{in}}}{\mathrm{d}t^q} = \pm\lambda R_d i(t)g(l) \tag{4}$$

where $R_d = R_{\text{off}} - R_{\text{on}}$. For linear window $g(l) = 1$ and using Riemann–Liouville Theorem [68] the memristor resistance can be derived as

$$R_{\text{in}} = \left(R_{\text{in}}^{q+1} \mp q(q+1)kR_d \int_0^t (t-\tau)^{q-1} v(\tau) \, \mathrm{d}\tau \right)^{\frac{1}{q+1}} \tag{5}$$

Similarly the memcapacitor can be derived from the relation

$$\begin{aligned} q_c(t) &= c_m(x, v, t)\, \omega(t) \\ \dot{x} &= f(x, v, t) \end{aligned} \tag{6}$$

where $q_c(t)$ is quantity of charge at time t, x is the correspondence internal state variable, and c_m is memcapacitor. The voltage across memcapacitor [66,67,69] is given by the relation

$$v(t) = c_m^{-1}(x, q_c, t)\, q_c(t) \tag{7}$$

c_m^{-1} is inverse memcapacitance.

Equations (6) and (7) can be simplified to a generalized forms as,

$$q(t) = c_m \left[\int_0^t v(\tau)\, \mathrm{d}\tau \right] v(t) \tag{8}$$

$$v(t) = c_m^{-1} \left[\int_0^t q(\tau)\, \mathrm{d}\tau \right] q(t) \tag{9}$$

Equation (8) is the voltage-controlled memcapacitance, and Eq. (9) is the charge-controlled memcapacitance.

Using Riemann–Liouville Theorem [68], the fractional-order model of (8) and (9) can be derived as

$$v(t) = \frac{c_m^{-1}}{\Gamma(q)} \left[\int_0^t (t-\tau)^{q-1} q(\tau)\, \mathrm{d}\tau \right] q(t) \tag{10}$$

$$q(t) = \frac{c_m}{\Gamma(q)} \left[\int_0^t (t-\tau)^{q-1} v(\tau)\, \mathrm{d}\tau \right] v(t) \tag{11}$$

Equation (10) shows the fractional-order charge controller memcapacitor and (11) shows the fractional-order voltage-controlled memcapacitor.

In this paper, we investigate a novel memfractor chaotic oscillator (MCO) with charge-controlled fracmemcapacitor (10) and flux-controlled fracmemristor (5) as shown in Fig. 1.

R is the resistance, L is the inductances, G is the conductance r is the internal resistance of the voltage source, and C is the capacitance. C_m is the fracmemcapacitor [66,67,69] and M is the flux-controlled memristor [66,67,69]. The current flowing through the circuit is i_G, i_R, i_{C_m}, i_L. The relationship between the voltage $v_{Cm}(t)$ and the charge $q_{Cm}(t)$ of the memcapacitor is defined as,

$$v_{Cm}(t) = (\alpha + \beta\sigma_{Cm})q_{Cm}(t) \tag{12}$$

Fig. 1 Memfractor chaotic oscillator
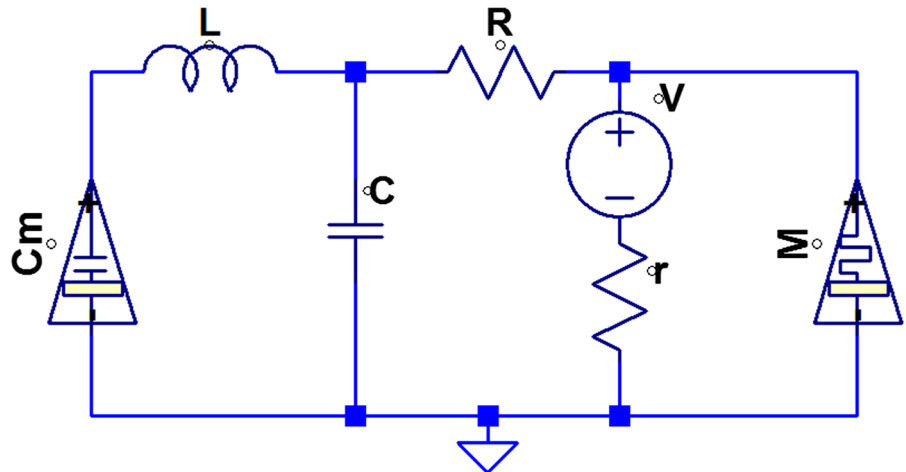
where $\frac{\mathrm{d}^{q_\sigma}\sigma}{\mathrm{d}t^{q_\sigma}} = q_{Cm}(t)$. Applying Kirchhoff's law to the circuit shown in Fig. 1, we derive the five state equations of the circuit as,

$$\frac{\mathrm{d}^{q_\sigma}\sigma}{\mathrm{d}t^{q_\sigma}} = q_{Cm}(t)$$

$$\frac{\mathrm{d}^{q_{qm}}q_M}{\mathrm{d}t^{q_{qM}}} = i_L$$

$$\frac{\mathrm{d}^{q_c}q_{c_m}}{\mathrm{d}t^{q_c}} = \frac{v_{Cm}}{r} + \frac{1}{R}(v_c + v_{Cm}) \qquad (13)$$

$$\frac{\mathrm{d}^{q_{i_L}}i_L}{\mathrm{d}t^{q_{i_L}}} = \frac{1}{L}(V_C - Mi_L)$$

$$\frac{\mathrm{d}^{q_{v_c}}v_c}{\mathrm{d}t^{q_{v_c}}} = \frac{1}{c}\left(-i_L + \frac{1}{R}(v_{Cm} - v_c)\right)$$

where $q_\sigma, q_{q_M}, q_{q_{Cm}}, q_{i_L}, q_{v_c}$ are the fractional orders of the MCO system. Using $x = \sigma, y = q_M, z = q_{Cm}, u = i_L, v = v_c$ and $e = \frac{1}{L}, f = \frac{1}{C}, g = \frac{1}{R}, h = \frac{1}{r}$, and with the memristor flux elements as $a = 0.01, b = 0.01$, memcapacitor charge control elements are $c = 0.7, d = -0.8$, the passive circuit elements are $L = 0.136H, C = 58.82F, R = 0.2\Omega$, and the internal resistance of the non-ideal voltage source is $r = 2.1\Omega$, we arrive at the fifth-order dimensionless mathematical model of the memfractor oscillator system as

$$\frac{\mathrm{d}^{q_x}x}{\mathrm{d}t^{q_x}} = z$$

$$\frac{\mathrm{d}^{q_y}y}{\mathrm{d}t^{q_y}} = u$$

$$\frac{\mathrm{d}^{q_z}z}{\mathrm{d}t^{q_z}} = a_1 z + a_2 xz + a_3 v \qquad (14)$$

$$\frac{\mathrm{d}^{q_u}u}{\mathrm{d}t^{q_u}} = a_4 v + a_5 u(1 + y)$$

$$\frac{\mathrm{d}^{q_v}v}{\mathrm{d}t^{q_v}} = a_6 u + a_7 xz + a_8 z + a_9 v + a_0$$

with $a_1 = -1.89; a_2 = -2.16; a_3 = 4.8; a_4 = 7.35; a_5 = -0.0735; a_6 = -0.17; a_7 = 0.6528; a_8 = 0.571; a_9 = -0.816$ and a_0 is model disturbance or the uncertainty in the model approximations. In this case, the value of $a_0 = 10^{-5}$ and the initial conditions are $[0, 0, 0, 0, 0.01]$. The parameter a_0 is the model uncertainty arising due to the voltage source and if the source is assumed to be an ideal voltage source (tolerance level less than 10^{-5}), then the disturbance factor $a_0 = 0$ and then the system is self-excited oscillator and if the voltage source is a non-ideal source with tolerance factor $a_0 \neq 0$, then the memfractor oscillator is a hidden attractor and thus the MCO system exhibits a chameleon [71,92] like behavior. Figure 2a, b shows the 2D phase portraits of the MCO system for $a_0 \neq 0$ and $a_0 = 0$, respectively.

3 Dynamic analysis of memfractor oscillator (MCO)

The dynamic properties of the MCO system such as dissipativity, equilibrium points, eigenvalues, Lyapunov exponents and Kaplan–Yorke dimension are derived and discussed in this section.
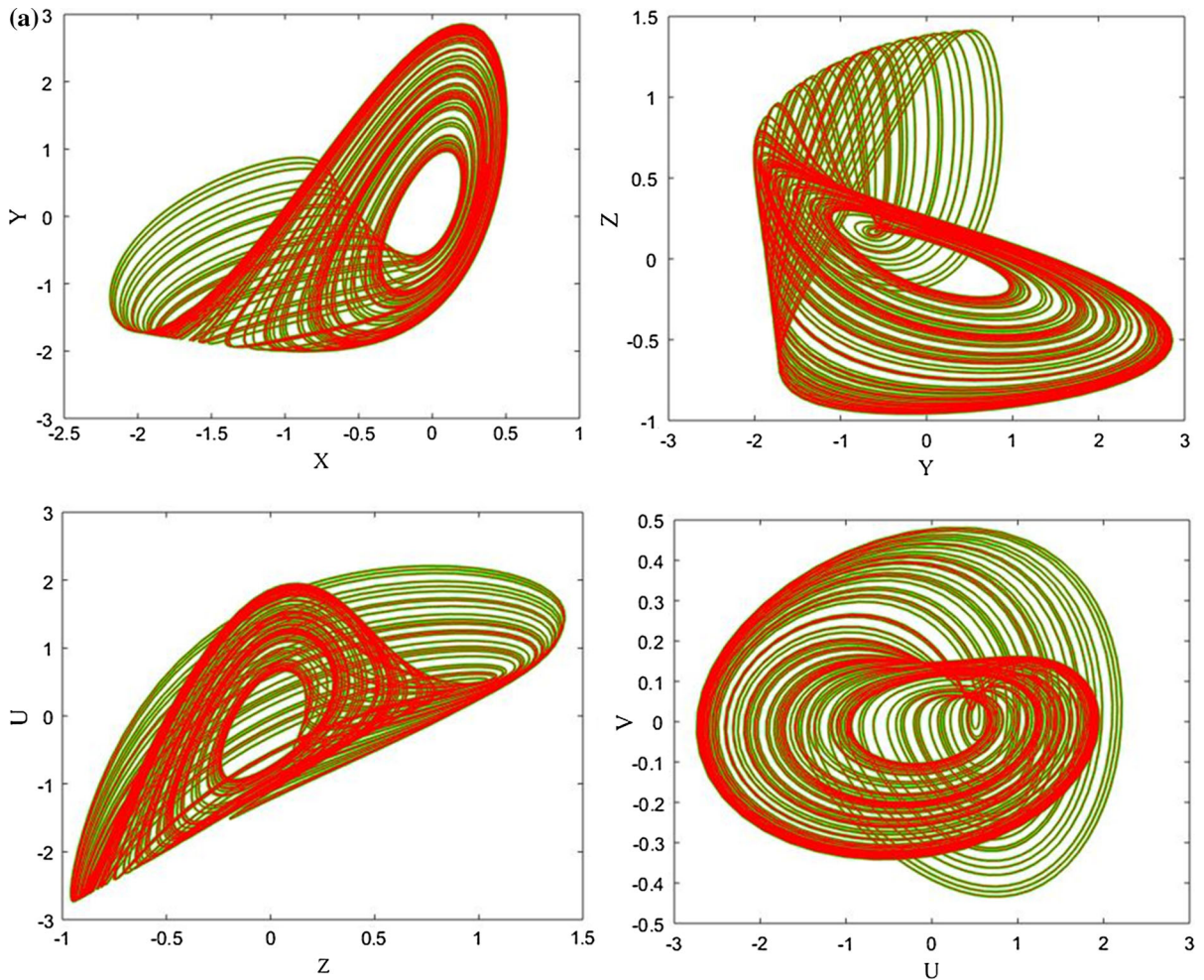
Fig. 2 **a** 2D phase portraits of the self-excited memfractor oscillator (14) for commensurate order $q = 0.993$. **b** 2D phase portraits of the hidden attractor memfractor oscillator (14) for commensurate order $q = 0.995$

3.1 Equilibrium points

The equilibrium points of the MCO system depend on the parameter a_0, and if $a_0 = 0$, the system is a self-excited attractor with one equilibrium point at origin (E_1). If $a_0 \neq 0$, the MCO system shows no equilibrium points and hence shows hidden attractors. The Jacobian matrix of the MCO system (3) is

$$J(X) = \begin{bmatrix} 0 & 0 & 1 & 0 & 0 \\ 0 & 0 & 0 & 1 & 0 \\ a_2 z & 0 & a_1 + a_2 x & 0 & a_3 \\ 0 & -a_5 u & 0 & a_5 - a_5 y & a_4 \\ a_7 z & 0 & a_8 + a_7 x & a_6 & a_9 \end{bmatrix}$$

(15)

3.2 Stability analysis

For the integer-order model of the MCO system (14) when the commensurate order of the system $q = 1$, the characteristic equation of the system is derived as,

$$\lambda^5 + (-a_1 - a_5 - a_9)\lambda^4 + \begin{pmatrix} a_1 a_5 + a_1 a_9 - a_4 a_6 \\ -a_3 a_8 + a_5 a_9 \end{pmatrix}\lambda^3 + \begin{pmatrix} a_1 a_4 a_6 - a_1 a_5 a_9 \\ +a_3 a_5 a_8 \end{pmatrix}\lambda^2 \quad (16)$$

and at equilibrium E_1 the characteristic equation is $\lambda^5 + 2.7795\lambda^4 + 0.248871\lambda^3 + 2.27339028\lambda^2$ and the corresponding eigenvalues are $\lambda_1 = -2.9555$, $\lambda_{2,3} = 0.0880 \pm 0.8726i$, $\lambda_{4,5} = 0$ and $\lambda_{2,3}$ is the saddle focus. As per Routh–Hurwitz criterion, all the principal minors need to be positive for the MCO system
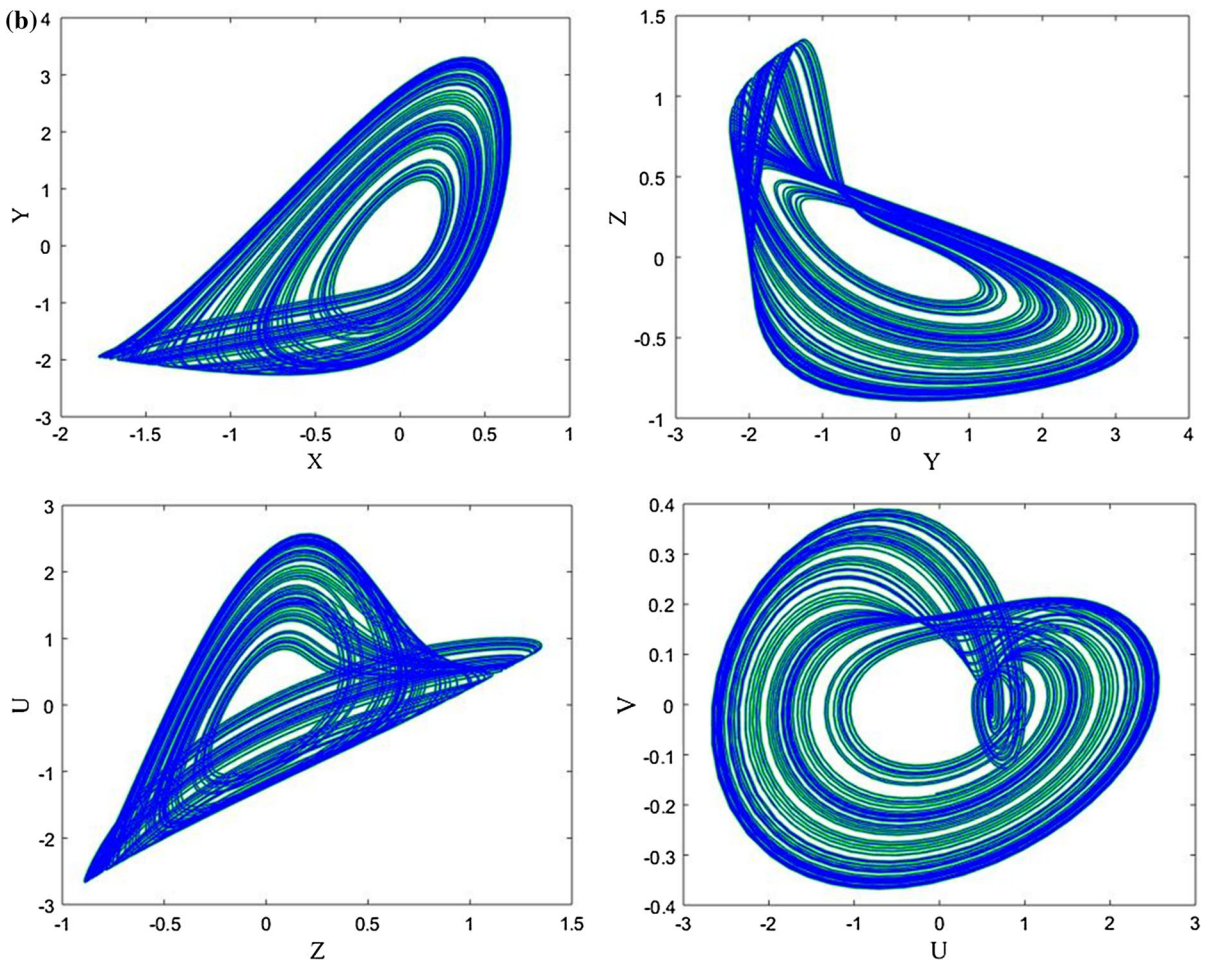
$\textcircled{\tiny 2}$ Springer

Fig. 2 continued

to be stable. The principal minors are,

$$\Delta_1 = \delta_1 > 0, \quad \Delta_2 = \begin{vmatrix} \delta_1 & \delta_0 \\ \delta_3 & \delta_2 \end{vmatrix} > 0,$$

$$\Delta_3 => \begin{vmatrix} \delta_1 & \delta_0 & 0 \\ \delta_3 & \delta_2 & \delta_1 \\ 0 & 0 & \delta_3 \end{vmatrix} > 0$$

$$\Delta_4 = \begin{vmatrix} \delta_1 & \delta_0 & 0 & 0 \\ \delta_3 & \delta_2 & \delta_1 & \delta_0 \\ 0 & \delta_4 & \delta_3 & \delta_2 \\ 0 & 0 & 0 & \delta_4 \end{vmatrix} > 0, \tag{17}$$

$$\Delta_5 = \begin{vmatrix} \delta_1 & \delta_0 & 0 & 0 & 0 \\ \delta_3 & \delta_2 & \delta_1 & \delta_0 & 0 \\ 0 & \delta_4 & \delta_3 & \delta_2 & \delta_1 \\ 0 & 0 & \delta_5 & \delta_4 & \delta_3 \\ 0 & 0 & 0 & 0 & \delta_5 \end{vmatrix} > 0$$

where $\delta_0 = 1, \delta_1 = -a_1 - a_5 - a_9, \delta_2 = a_1 a_5 + a_1 a_9 - a_4 a_6 - a_3 a_8 + a_5 a_9, \delta_3 = a_1 a_4 a_6 - a_1 a_5 a_9 + a_3 a_5 a_8 \delta_4 = 0, \delta_5 = 0$. For the parameter values of $a_1 = -1.89; a_2 = -2.16; a_3 = 4.8; a_4 = 7.35; a_5 = -0.0735; a_6 = -0.17; a_7 = 0.6528; a_8 = 0.5712; a_9 = -0.816$ and at the equilibrium point E_1 the MCO system is unstable and shows chaotic oscillations. The system characteristic equation does not depend on the value of a_0, and hence, the eigenvalues are same for self-excited and hidden chaotic flows. Similarly the fractional-order stability analysis is also same for self-excited and hidden flows, and hence, Theorems 1–3 are common for both $a_0 = 0$ and $a_0 \neq 0$

Theorem 1 *The commensurate order system $D^q x(t) = Ax(t)$, with $0 < q \leq 1$ and $x(t) \in R^n$, $A \in R^{n \times n}$ is asymptotically stable if and only if $|\arg(\lambda)| > \frac{q\pi}{2}$ for*

all eigenvalues of λ. *For the critical eigenvalues, the system is stable if* $|\arg(\lambda)| \geq \frac{q\pi}{2}$ *where the critical eigenvalue of* $|\arg(\lambda)| = \frac{q\pi}{2}$ *having geometric multiplicity of one.*

Proof For commensurate MCO system of order q, the system is stable and exhibits chaotic oscillations if $|\arg(eig(J_E))| = |\arg(\lambda_i)| > \frac{q\pi}{2}$ where J_E is the Jacobian matrix at the equilibrium E and λ_i are the eigenvalues of the MCO system where $i = 1, 2, 3, 4, 5$. As seen from the MCO system, the eigenvalues should remain in the unstable region and the necessary condition for the MCO system to be stable is $q > \frac{2}{\pi} \tan^{-1}\left(\frac{|Im\lambda|}{Re\lambda}\right)$. The characteristic equation for the commensurate orders $q = 0.99$ for the equilibrium point E_1 is given by

$$\lambda^{495} + 5\lambda^{397} + 2.77\lambda^{396} + 10\lambda^{299} + 11.19\lambda^{298}$$
$$+ 0.25\lambda^{297} + 10\lambda^{201} + 16.67\lambda^{200} + 0.75\lambda^{199}$$
$$+ 2.27\lambda^{198} + 5\lambda^{103} + 11.19\lambda^{102} + 0.746\lambda^{101}$$
$$+ 4.546\lambda^{100} + \lambda^5 + 2.779\lambda^4 + 0.248\lambda^3 + 2.273\lambda^2.$$

$\square$

Theorem 2 *For incommensurate order system* $D^q x(t) = Ax(t)$, $q = \left(q_x, q_y, q_z, q_u, q_v\right)^T$ *with* $q_i = \frac{num(i)}{den(i)}$ *and* $\gcd(num(i), den(i)) = 1$ *for* $i = x, y, z, u, v$ *and if 'M' is* $LCM(den(i))$, *then the system is globally asymptotically stable if all the eigenvalue of the system obeys* $|\arg(\lambda)| > \frac{\pi}{2m}$ *where* $\Delta(\lambda) = \det\left(diag(\lambda^{Mq_i}) - A\right) = 0$

Proof The necessary condition for the MCO system to exhibit chaotic oscillations in the incommensurate case is, $\frac{\pi}{2M} - \min_i\left(|\arg(\lambda_i)|\right) > 0$ where M is the LCM of the fractional orders. If $q_x = 0.99, q_y = 0.99, q_z = 0.99, q_u = 0.98, q_v = 0.98$, then $M = 100$. The characteristic equation of the system evaluated at the equilibria is $\det(diag[\lambda^{Mq_x}, \lambda^{Mq_y}, \lambda^{Mq_z}, \lambda^{Mq_u}, \lambda^{Mq_v}] - J_E) = 0$ and by substituting the values of M and the fractional orders, $\det(diag[\lambda^{99}, \lambda^{99}, \lambda^{99}, \lambda^{98}, \lambda^{98}] - J_E) = 0$ and the characteristic equation at equilibrium point E_1 is,

$$\lambda^{493} + 2\lambda^{396} + 3.889\lambda^{395} + 1.89\lambda^{394} + \lambda^{299}$$
$$+ 6.8895\lambda^{298} + 10.757\lambda^{297} + 2.719\lambda^{296} + 3\lambda^{201}$$
$$+ 10.558\lambda^{200} + 14.096\lambda^{199} + 2.042\lambda^{198} + 3\lambda^{103}$$
$$+ 8.44\lambda^{102} + 6.47\lambda^{101} + 3.48\lambda^{100} + \lambda^5$$
$$+ 2.779\lambda^4 + 0.248871\lambda^3 + 2.273\lambda^2.$$

For the values of parameters mentioned in Sect. 2, the approximated solution of the characteristic equation is $\lambda_{493} = 0.677$, whose argument is zero and which is the minimum argument, and hence, the stability necessary condition becomes, $\frac{\pi}{200} - 0 > 0$ which solves for $0.0157 > 0$ and hence the MCO system is unstable and chaos exists in the incommensurate system. $\square$

Theorem 3 *The necessary condition for occurrence of a chaotic attractor in the fractional-order system* (14) *for* $a = 0$ *is* $q > \frac{2}{\pi} \arctan\left(\frac{|Im(\lambda)|}{Re(\lambda)}\right)$ *for any eigenvalue* λ *of the equilibrium point.*

Proof The MCO system shows chaotic oscillations and has $\lambda_{2,3}$ saddle focus. A necessary condition for the MCO system to exhibit a chaotic attractor is instability of the equilibrium point E_1. Otherwise, the equilibrium point becomes asymptotically stable and attracts the nearby trajectories. By Theorem 3, the condition for instability of equilibrium is $q > \frac{2}{\pi} \arctan\left(\frac{|Im(\lambda)|}{Re(\lambda)}\right)$ and from the saddle focus $\lambda_{2,3}$ chaotic oscillations exists when $q > \frac{2}{\pi} \arctan\left(\frac{|0.8726|}{0.088}\right)$ and the minimum value of $q = 0.936$ above which the system shows chaotic oscillations. $\square$

3.3 Lyapunov exponents and Kaplan–Yorke dimension

Lyapunov exponents of a nonlinear system define the convergence and divergence of the states. The existence of a positive Lyapunov exponents confirms the chaotic behavior of the system [45,57–60]. Lyapunov exponents (LEs) are necessary and more convenient for detecting hyperchaos in fractional-order hyperchaotic system. A definition of LEs for fractional differential systems was given in [57] based on frequency-domain approximations, but the limitations of frequency-domain approximations are highlighted by Tavazoei [45]. Time series-based LEs calculation methods like Wolf algorithm [58], Jacobian method [59] and neural network algorithm [60] are popularly known ways of calculating Lyapunov exponents for integer- and fractional-order systems. To calculate the LEs of the MCO system, we use the Lyapunov exponents for fractional order using Wolf's algorithm [70].

Fig. 3 Lyapunov exponents of the MCO system. **a** $a_0 = 0$, **b** $a_0 \neq 0$
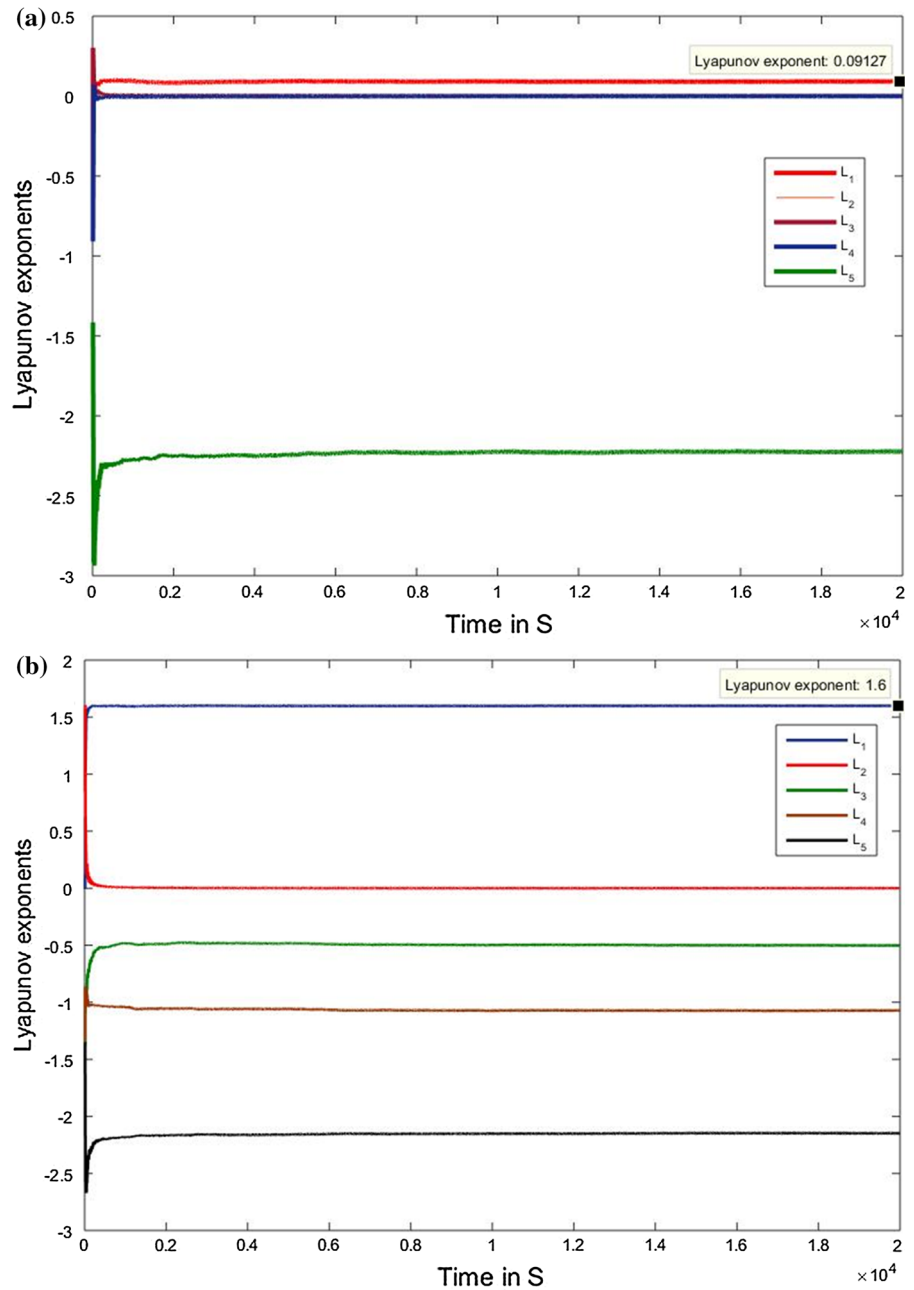
The Lyapunov exponents of the MCO system for $a_0 = 0$ are numerically found as

$$L_1 = 0.09127, \ L_{2,3,4} = 0, \ L_5 = -2.2236 \quad (18)$$

and Lyapunov exponents of the MCO system for $a_0 \neq 0$ are numerically found as

$$L_1 = 1.6, \ L_2 = 0, \ L_3 = -0.521,$$
$$L_4 = -1.076, \ L_5 = -2.2311 \quad (19)$$

The existence of positive LE confirms that the MCO system shows chaotic oscillations for both self-excited (18) and hidden attractor (19). Figure 3a, b shows the time history of Lyapunov exponents of MCO system for $a_0 = 0$ and $a_0 \neq 0$.

We note that the sum of the Lyapunov exponents of the MCO system (14) is negative. In fact,

$$a = 0 \Rightarrow L_1 + L_{2,3,4} + L_5 = -2.1323 < 0$$
$$a \neq 0 \Rightarrow L_1 + L_2 + L_3 + L_4 + L_5 = -2.2271 < 0$$
(20)

This shows that the MCO system (14) is dissipative.

Also, the Kaplan–Yorke dimension of the MCO system (14) is derived as

$$a = 0 \Rightarrow D_{KY} = 4 + \frac{L_1 + L_{2,3,4}}{|L_5|} = 4.042,$$
$$a \neq 0 \Rightarrow D_{KY} = 4 + \frac{L_1 + L_{2,3,4}}{|L_5|} = 4.002,$$
(21)

which is fractional.

3.4 Bifurcation

3.4.1 Bifurcation with parameters

To understand the parameter dependence of the MCO system, we derive and investigate the bifurcation plots. This MCO system bifurcates with all the six parameters. Figure 4a–j shows the bifurcation of the MCO system for the parameters $a_1, a_2, a_3, a_4, a_5, a_6, a_7, a_8, a_9, a_0$, respectively. From Fig. 4a–j, it is evident that the MCO system shows multiple chaotic regions for parameters. The system enters into chaotic oscillations with routine period doubling or reverse period doubling exit from chaos. Figure 4a shows the bifurcation of the MCO with parameter a_1, and the MCO shows period 8 limit cycles for $-2 \leq a_1 < -1.96$ and enters into the chaotic region with multiple period doublings and similarly the MCO shows period 8 limit cycles for $-1.9 \leq a_2 < -1.8$, period 4 limit cycles for $-1.8 \leq a_2 < -1.4$ and period 2 limit cycles for $-1.4 \leq a_2 < -1$ and takes a period halving exit from chaos as shown in Fig. 4b. Figure 4c shows the bifurcation of the MCO with a_3 and has period 4, period 8 and chaotic oscillations for $4.5 \leq a_3 < 4.59, 4.59 \leq a_3 < 4.61, 4.61 \leq a_3 < 4.85$, respectively, and takes period doubling route to crisis. Similarly the parameters a_5, a_6, a_8, a_9 take period doubling route to chaos, and a_4, a_7, a_0 take the inverse period doubling exit from chaos. These claims are supported by the respective Lyapunov exponents as shown in Fig. 5. Two Lyapunov exponents are zero, two are negative, and one Lyapunov

exponent is positive confirming the existence of chaotic oscillations.

3.4.2 Bifurcation with fractional order

The most important analysis of interest when investigating a fractional-order system is the bifurcation with fractional order. Figure 6a, b shows the bifurcation of the MCO system with fractional order for $a = 0$ and $a \neq 0$, respectively. As can be seen from Fig. 6a, b, bifurcation of the MCO system for change in fractional order shows that the systems chaotic oscillations remain if $q_i > 0.93$ and the largest positive Lyapunov exponent ($L_1 = 0.1024$) of the MCO system for $a = 0$ appears when $q = 0.995$ against its largest integer-order Lyapunov exponent ($L_1 = 0.09127$) and the largest positive Lyapunov exponent ($L_1 = 1.6582$) of the MCO system for $a \neq 0$ appears when $q = 0.993$ against its largest integer-order Lyapunov exponent ($L_1 = 1.6$).

3.5 Bicoherence

Higher-order spectra have been used to study the nonlinear interactions between frequency modes [38,39]. Let $x(t)$ be a stationary random process defined as,

$$x(t) = \sum_{n=1}^{N} A_n e^{j\omega_n t} + A_n^* e^{-j\omega_n t}$$
(22)

where ω is the angular frequency, n is the frequency modal index, and A_n are the complex Fourier coefficients. The power spectrum can be defined as,

$$P(\omega_k) = E[A_{\omega_k} A_{\omega_k}^*]$$
(23)

and discrete bispectrum can be defined as,

$$B(\omega_k, \omega_j) = E\left[A_{\omega_k} A_{\omega_j} A_{\omega_k + \omega_j}^*\right]$$
(24)

If the modes are independent, then the average triple products of Fourier components are zero resulting in a zero bispectrum [38]. The study of bicoherence is to give an indication of the relative degree of phase coupling between triads of frequency components. The motivation to study the bicoherence is twofold. First, the bicoherence can be used to extract information
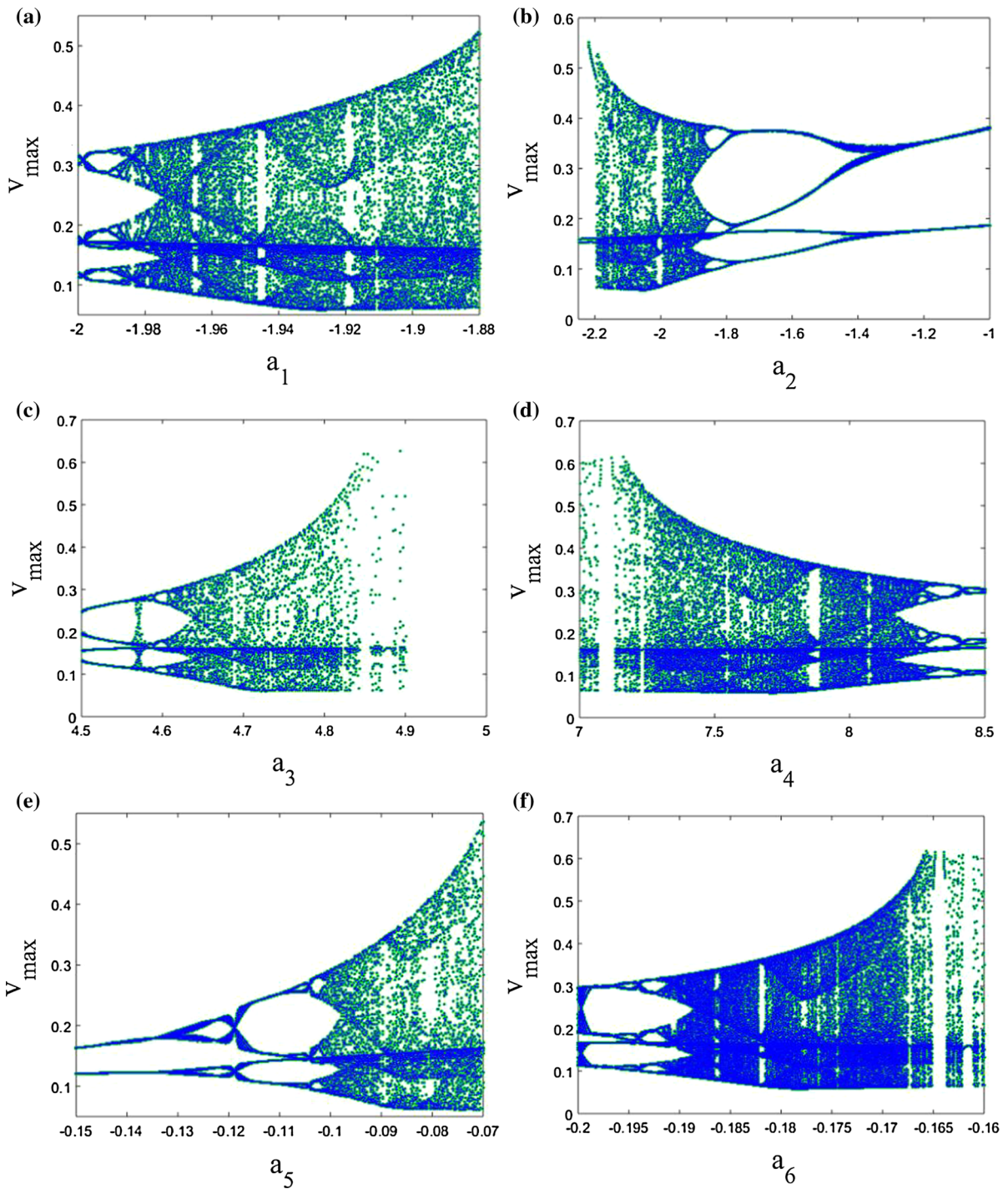
Fig. 4 Bifurcation plots of MCO system

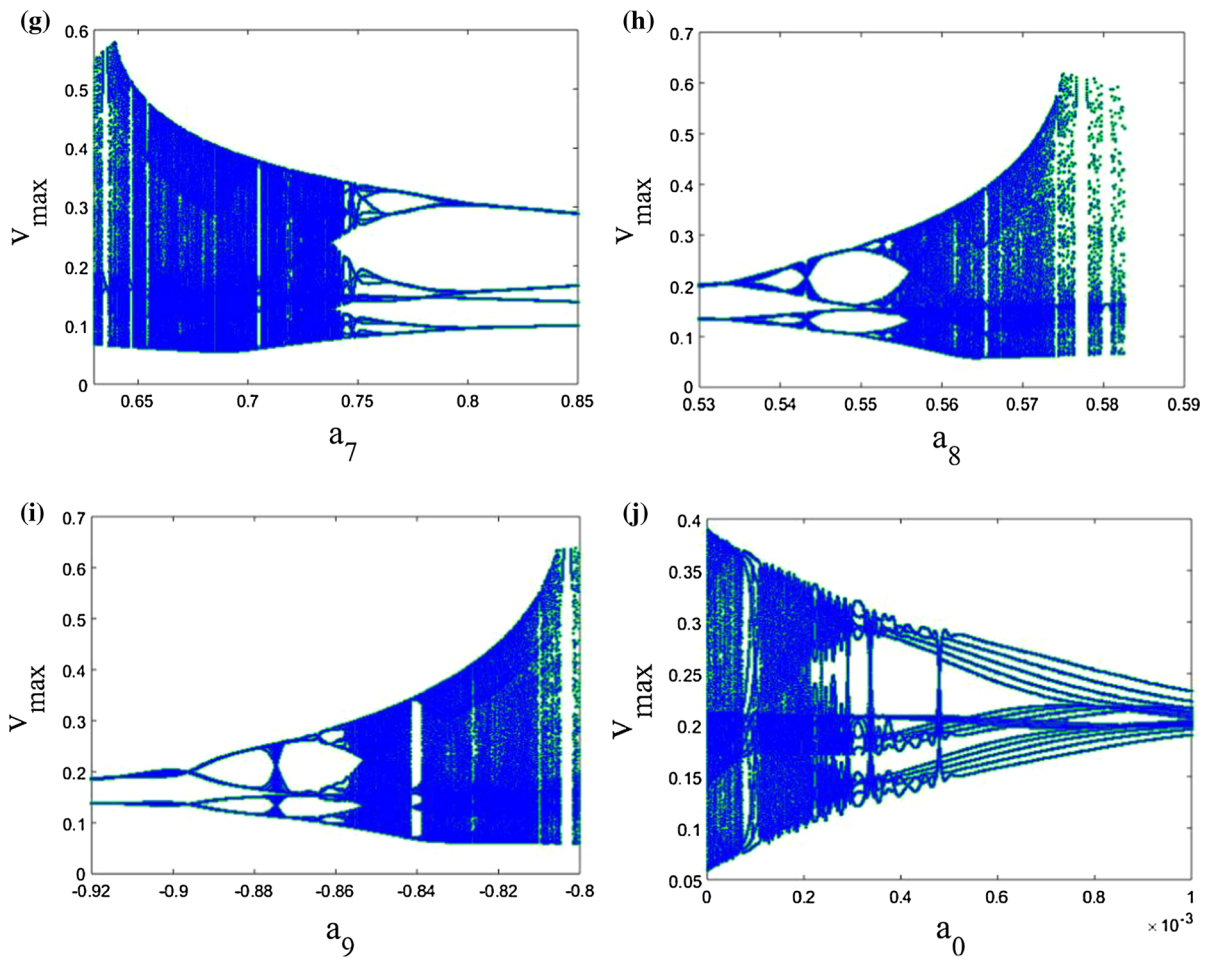**(g)**

(h)

(i)

(j)

Fig. 4 continued

due to deviations from Gaussianity and suppress additive (colored) Gaussian noise. Second, the bicoherence can be used to detect and characterize asymmetric nonlinearity in signals via quadratic phase coupling or identify systems with quadratic nonlinearity. The bicoherence is the third-order spectrum. Whereas the power spectrum is a second-order statistics, formed from $X'(f)^* X(f)$, where $X(f)$ is the Fourier transform of $x(t)$, the bispectrum is a third-order statistics formed from $X(f_j) * X(f_k) * X'(f_j + f_k)$. The bispectrum is therefore a function of a pair of frequencies (f_j, f_k). It is also a complex-valued function. The (normalized) square amplitude is called the bicoherence (by analogy with the coherence from the cross-spectrum).The bispectrum is calculated by dividing the time series into M segments of length N_seg, calculating their Fourier transforms and bi-periodogram, then

averaging over the ensemble. Although the bicoherence is a function of two frequencies, the default output of this function is a one-dimensional output, the bicoherence refined as a function of only the sum of the two frequencies. The auto-bispectrum of a chaotic system is given by Pezeshki [30]. He derived the auto-bispectrum with the Fourier coefficients.

$$B(\omega_1, \omega_2) = E[A(\omega_1) A(\omega_2) A^*(\omega_1 + \omega_2)] \qquad (25)$$

where ω_n is the radian frequency and A is the Fourier coefficients of the time series. The normalized magnitude spectrum of the bispectrum known as the squared bicoherence is given by

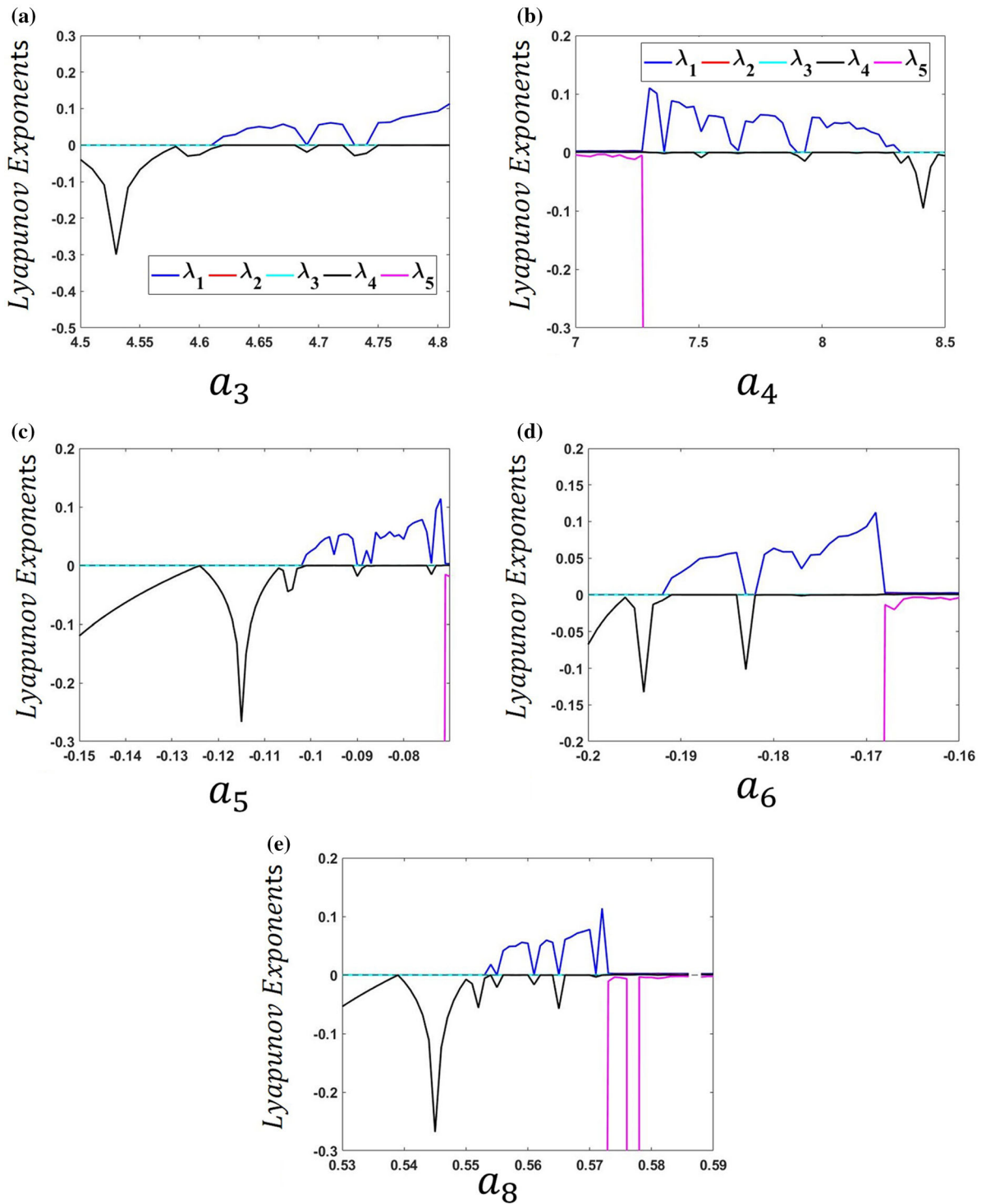$$b(\omega_1, \omega_2) = |B(\omega_1, \omega_2)|^2 / P(\omega_1) P(\omega_2) P(\omega_1 + \omega_2)$$
$$(26)$$

Fig. 5 Change in Lyapunov exponents of MCO system for various values of parameters (The fifth Lyapunov exponent is not visible in the plots 5**b**–5**e** and fourth and fifth Lyapunov exponents are not visible in plot 5**a**)
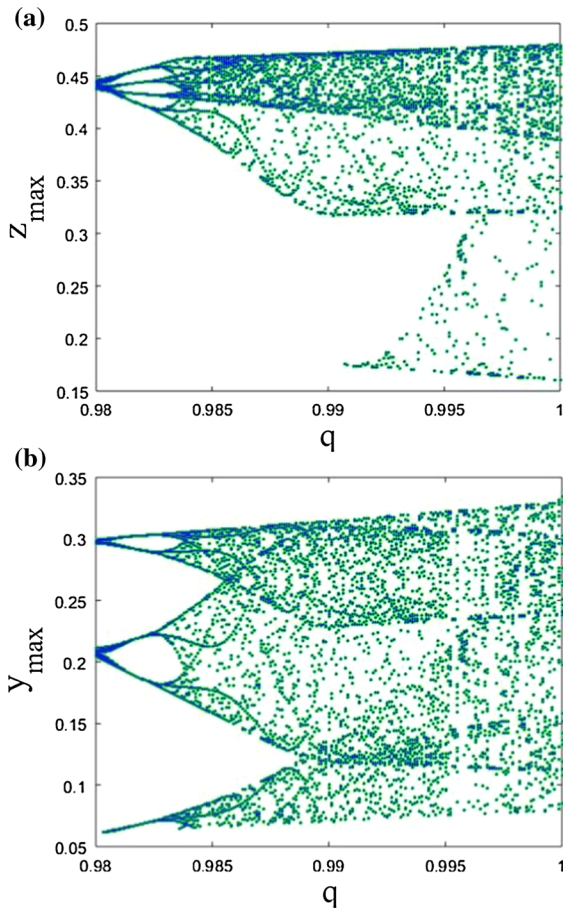
(a)

(b)

Fig. 6 **a** Bifurcation of MCO system ($a = 0$) with fractional order. **b** Bifurcation of MCO system ($a \neq 0$) with fractional order

where $P(\omega_1)$ and $P(\omega_2)$ are the power spectra at f_1 and f_2.

Figures 7a, b and 8a, b show the bicoherence contours of the MCO system for state x and all states together with $a = 0$ and $a \neq 0$, respectively. Shades in yellow represent the multifrequency components contributing to the power spectrum. From Figs. 7a, b and 8a, b, the cross-bicoherence is significantly nonzero and non-constant, indicating a nonlinear relationship between the states. As can be seen from Fig. 7a, b, the spectral power is very low as compared to the spectral power of all states together (Fig. 8a, b) indicating the existence of multifrequency nodes. Also Fig. 8a, b shows the nonlinear coupling (straight lines connecting multiple frequency terms) between the states. The yellow shades/lines and non-sharpness of the peaks, as well as the presence of structure around

the origin in figures (cross-bicoherence), indicate that the nonlinearity between the states x, y, z, u, v is not of the quadratic nonlinearity and hence may be because of nonlinearity of higher dimensions. The most two dominant frequencies (f_1, f_2) are taken for deriving the contour of bicoherence. The sampling frequency (f_s) is taken as the reference frequency. Direct FFT is used to derive the power spectrum for individual frequencies, and Hankel operator is used as the frequency mask. Hanning window is used as the FIR filter to separate the frequencies [40].

4 FPGA implementation of the MCO systems

The three main approaches derived to solve fractional-order chaotic systems are frequency-domain method [42], Adomian decomposition method (ADM) [43] and Adams–Bashforth–Moulton (ABM) algorithm [44]. The frequency-domain method is not always reliable in detecting chaos behavior in nonlinear systems [45]. On the other hand, ABM and ADM are more accurate and convenient to analyze dynamical behaviors of a nonlinear system. Compared with the ABM, ADM yields more accurate results and needs less computing resources as well as memory resources [46]. Hence, the proposed MCO system is implemented in FPGA by applying ADM scheme. The challenge of implementing the systems in FPGA is designing the fractional-order integrator which is not a readily available block in the system generator [18,40,41]. As because the ADM algorithm converges fast [46,47], the first 6 terms are used to get the solution of MCO system as in real cases, it is impossible to find the accurate value of x when t takes larger values [48]. Hence, we have to design a time discretization method. That is to say, for a time interval of t_i (initial time) to t_f (final time), we divide the interval into (t_n, t_{n+1}) and we get the value of $x(n + 1)$ at time t_{n+1} by applying $x(n)$ at time t_n using the relation $x(n + 1) = F(x(n))$ [48]. We use the ADM method [55,58] to discretize the fractional-order CA system for implementing in FPGA using the hardware–software cosimulation as described in [85,86]. The fractional-order discrete form of the dimensionless state equations for the MCO system can be given as,

Fig. 7 **a** Bicoherence plot of MCO system ($a = 0$) for state x. **b** Bicoherence plot of MCO system ($a \neq 0$) for state x
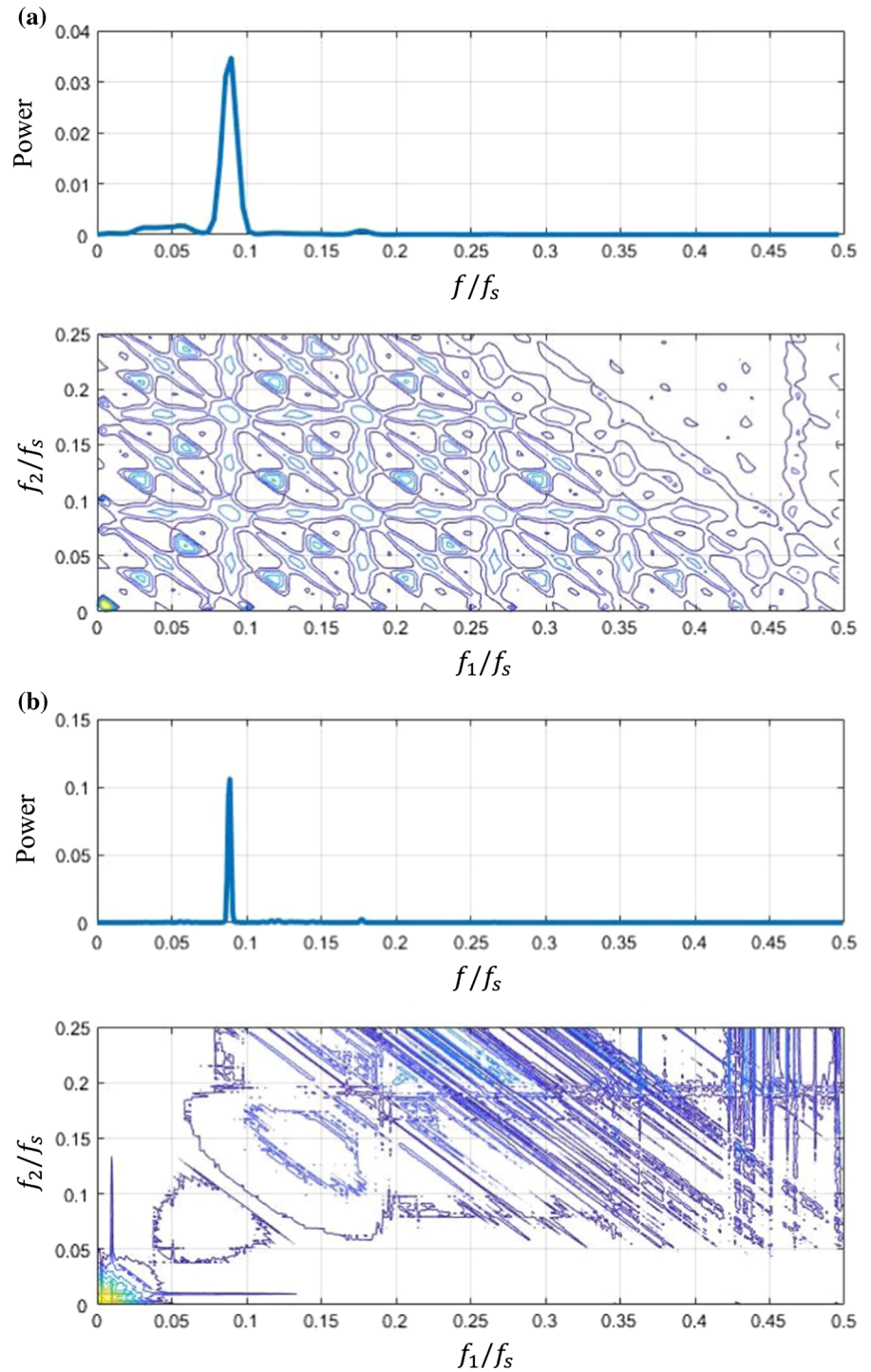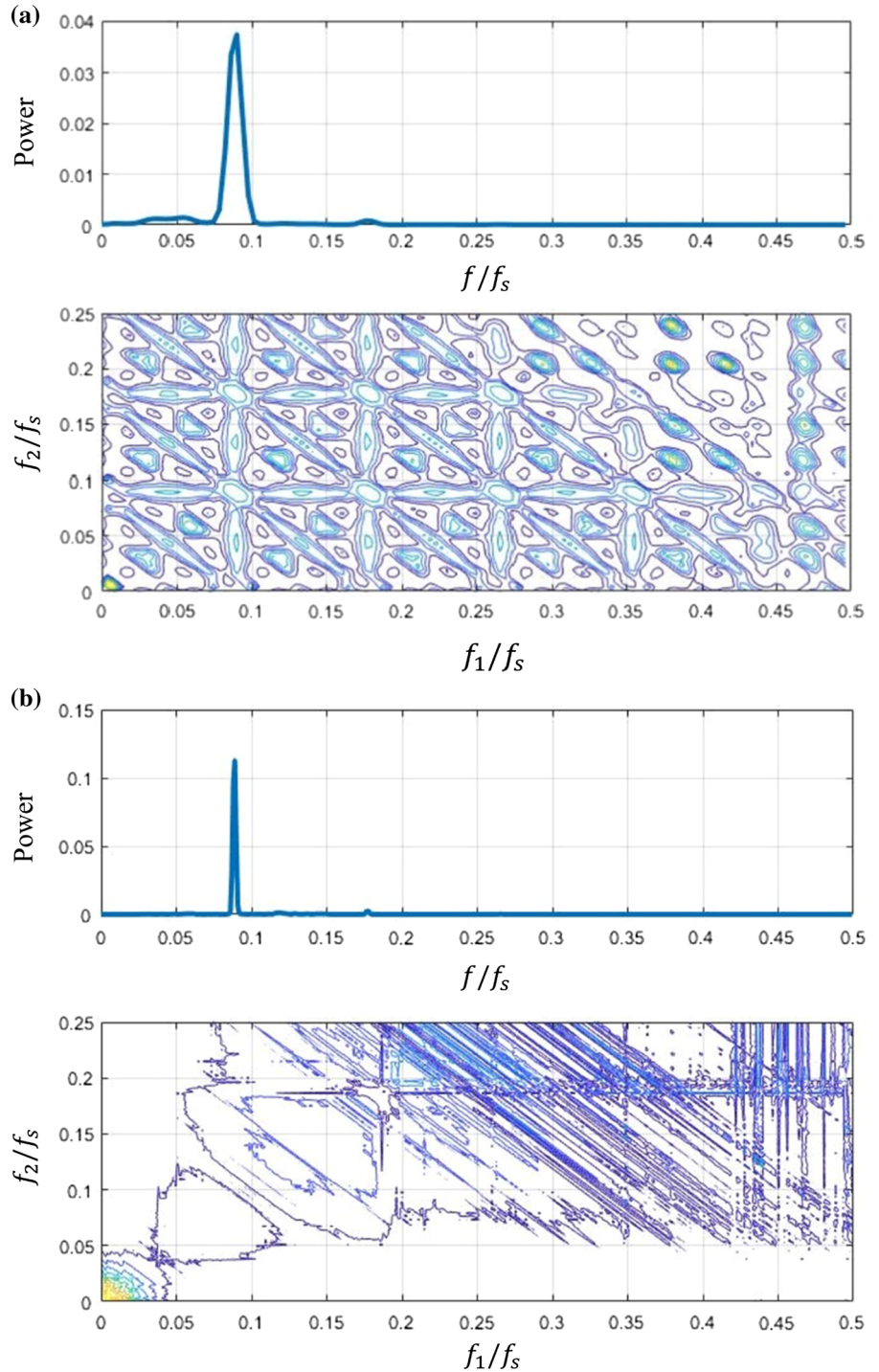
Fig. 8 **a** Bicoherence plot of MCO system ($a = 0$) for all states. **b** Bicoherence plot of MCO system ($a \neq 0$) for all states
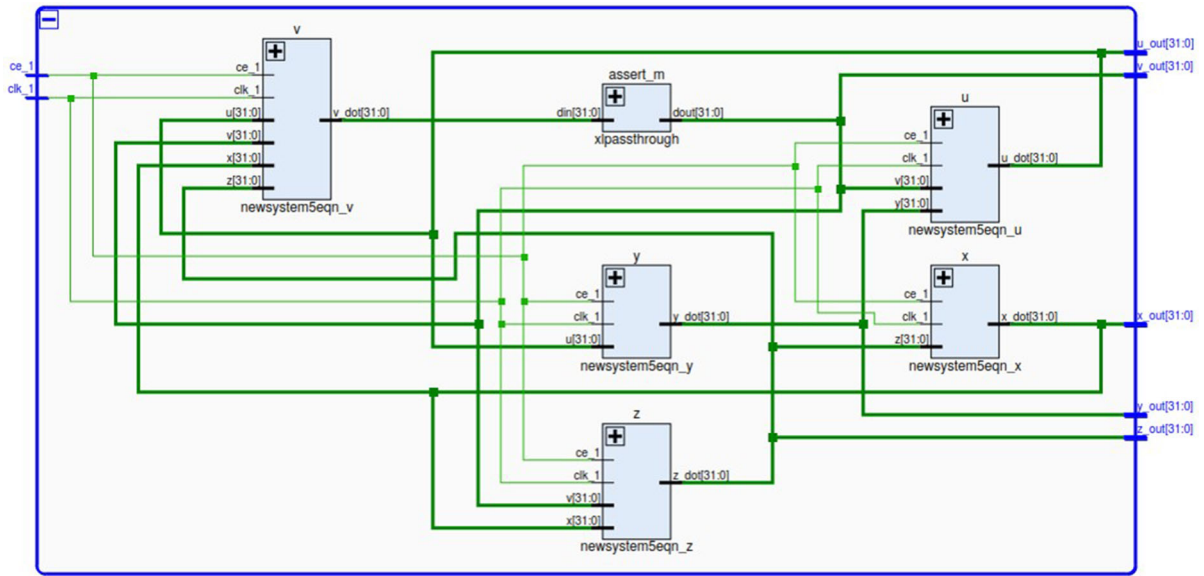
Fig. 9 RTL schematics of the MCO system implemented in Kintex 7 (Device = 7k160t Package = fbg484 S). The sampling time of the system is kept at 0.01s to minimize the time slack errors. The entire system is configured for a 32bit operation
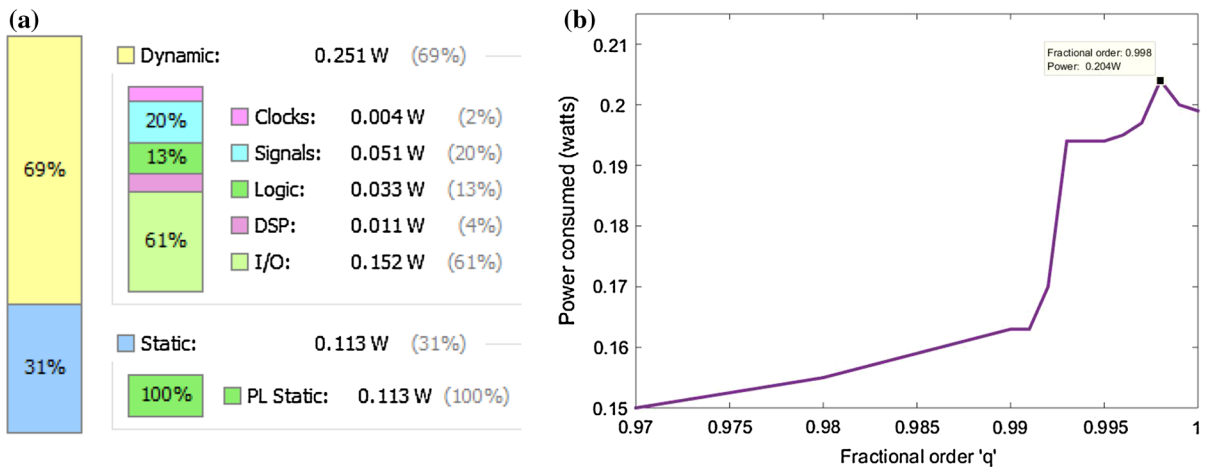

Fig. 10 a Power consumed by MCO system ($a = 0$) for $q = 0.995$. **b** Power consumed by MCO system for various fractional orders. It can be seen that maximum power of 0.251W is consumed for order $q = 0.995$ when the MCO system shows the largest Lyapunov exponents

$$x_{n+1} = \sum_{j=0}^{6} p_1^j \frac{h^{jq_x}}{\Gamma(jq_x + 1)}$$

$$y_{n+1} = \sum_{j=0}^{6} p_2^j \frac{h^{jq_y}}{\Gamma(jq_y + 1)}$$

$$z_{n+1} = \sum_{j=0}^{6} p_3^j \frac{h^{jq_z}}{\Gamma(jq_z + 1)} \tag{27}$$

$$u_{n+1} = \sum_{j=0}^{6} p_4^j \frac{h^{jq_u}}{\Gamma(jq_u + 1)}$$

$$v_{n+1} = \sum_{j=0}^{6} p_5^j \frac{h^{jq_v}}{\Gamma(jq_v + 1)}$$

where p_i^j are the Adomian polynomials with $i = 1, 2, 3, 4$ and

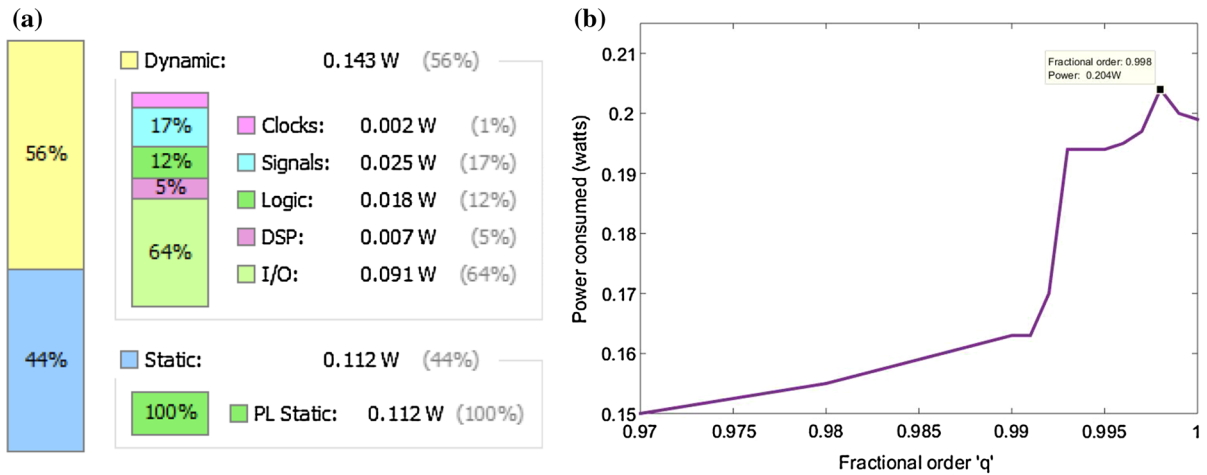$$p_1^0 = x_n, \; p_2^0 = y_n, \; p_3^0 = z_n, \; p_4^0 = u_n, \; p_5^0 = v_n$$

Fig. 11 a Power consumed by MCO system ($a \neq 0$) for $q = 0.993$. **b** Power consumed by MCO system for various fractional orders. It can be seen that maximum power of 0.251W is consumed for order $q = 0.993$ when the MCO system shows the largest Lyapunnov exponents

The Adomian first polynomial is derived as,

$$
\begin{aligned}
p_1^1 &= p_3^0 \\
p_2^1 &= p_4^0 \\
p_3^1 &= a_1 p_3^0 + a_2 p_1^0 p_3^0 + a_3 p_5^0 \\
p_4^1 &= a_4 p_5^0 + a_5 p_4^0 + a_5 p_4^0 p_2^0 \\
p_5^1 &= a_6 p_4^0 + a_7 p_1^0 p_3^0 + a_8 p_3^0 + a_9 p_5^0 + a_0
\end{aligned}
\tag{28}
$$

The Adomian second polynomial is derived as,

$$
\begin{aligned}
p_1^2 &= p_3^1 \\
p_2^2 &= p_4^1 \\
p_3^2 &= a_1 p_3^1 + a_2 \left[p_1^0 p_3^1 + p_1^1 p_3^0 \right] + a_3 p_5^1 \\
p_4^2 &= a_4 p_5^1 + a_5 p_4^1 + a_5 \left[p_4^1 p_2^0 + p_4^0 p_2^1 \right] \\
p_5^2 &= a_6 p_4^1 + a_7 \left[p_1^0 p_3^1 + p_1^1 p_3^0 \right] a_8 p_3^1 + a_9 p_5^1 + a_0
\end{aligned}
\tag{29}
$$

The Adomian third polynomial is derived as,

$$
\begin{aligned}
p_1^3 &= p_3^2 \\
p_2^3 &= p_4^2 \\
p_3^3 &= a_1 p_3^2 + a_2 \left[p_1^2 p_3^0 + p_1^0 p_3^2 + \frac{\Gamma(2q_z+1)}{\Gamma^2(q_z+1)} p_1^1 p_3^1 \right] + a_3 p_5^2 \\
p_4^3 &= a_4 p_5^2 + a_5 p_4^2 + a_5 \left[p_4^2 p_2^0 + p_4^0 p_2^2 + \frac{\Gamma(2q_u+1)}{\Gamma^2(q_u+1)} p_4^1 p_2^1 \right] \\
p_5^3 &= a_6 p_4^2 + a_7 \left[p_1^2 p_3^0 + p_1^0 p_3^2 + \frac{\Gamma(2q_v+1)}{\Gamma^2(q_v+1)} p_1^1 p_3^1 \right] \\
&\quad + a_8 p_3^2 + a_9 p_5^2 + a_0
\end{aligned}
\tag{30}
$$

Table 1 Resource consumption of FPGA-implemented MCO system for $a = 0$

Resource	Utilization	Available	Utilization %
LUT	2361	101,400	2.33
FF	518	202,800	0.26
DSP	12	600	2.00
IO	161	285	56.49
BUFG	1	32	3.13

Table 2 Resource consumption of FPGA-implemented MCO system for $a \neq 0$

Resource	Utilization	Available	Utilization %
LUT	2361	101,400	2.33
FF	518	202,800	0.26
DSP	12	600	2.00
IO	161	285	56.49
BUFG	1	32	3.13

The Adomian fourth polynomial is derived as,

$$
\begin{aligned}
p_1^4 &= p_3^3 \\
p_2^4 &= p_4^3 \\
p_3^4 &= a_1 p_3^3 \\
&\quad + a_2 \left[p_1^3 p_3^0 + p_1^0 p_3^3 \right.
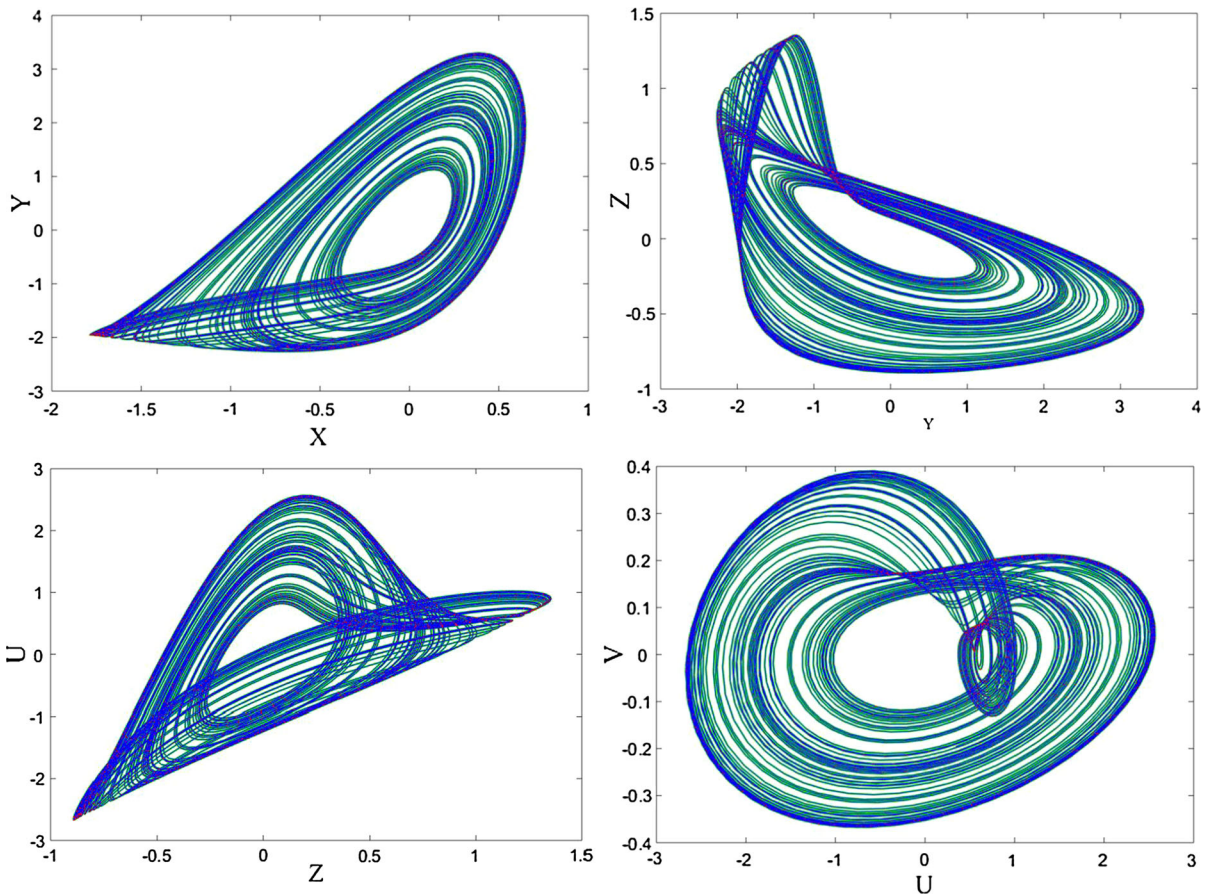\end{aligned}
$$

Fig. 12 2D phase portraits of the FPGA-implemented MCO system for $a = 0$. The initial conditions and parameter values are taken as in Sect. 2, and the order of the system is $q = 0.995$

$$+ \frac{\Gamma(3q_z + 1)}{\Gamma(q_z + 1)\Gamma(2q_z + 1)} \left[p_1^2 p_3^1 + p_1^1 p_3^2 \right] \Bigg]$$

$$+ a_3 p_5^3$$

$$p_4^4 = a_4 p_5^3 + a_5 p_4^3$$

$$+ a_5 \left[p_4^3 p_2^0 + p_4^0 p_2^3 \right]$$

$$+ \frac{\Gamma(3q_u + 1)}{\Gamma(q_u + 1)\Gamma(2q_u + 1)} \left[p_4^2 p_2^1 + p_4^1 p_2^2 \right] \Bigg]$$

$$p_5^4 = a_6 p_4^3$$

$$+ a_7 \left[p_1^3 p_3^0 + p_1^0 p_3^3 \right]$$

$$+ \frac{\Gamma(3q_v + 1)}{\Gamma(q_v + 1)\Gamma(2q_v + 1)} \left[p_1^2 p_3^1 + p_1^1 p_3^2 \right] \Bigg]$$

$$+ a_8 p_3^3 + a_9 p_5^3 + a_0 \tag{31}$$

The Adomian fifth polynomial is derived as,

$$p_1^5 = p_3^4$$

$$p_2^5 = p_4^4$$

$$p_3^5 = a_1 p_3^4$$

$$+ a_2 \left[p_1^4 p_3^0 + p_1^0 p_3^4 \right]$$

$$+ \frac{\Gamma(4q_z + 1)}{\Gamma(q_z + 1)\Gamma(3q_z + 1)} \left[p_1^3 p_3^1 + p_1^1 p_3^3 + p_1^2 p_3^2 \right] \Bigg]$$

$$+ a_3 p_5^4$$

$$p_4^5 = a_4 p_5^4 + a_5 p_4^4$$

$$+ a_5 \left[p_4^4 p_2^0 + p_4^0 p_2^4 \right]$$

$$+ \frac{\Gamma(4q_u + 1)}{\Gamma(q_u + 1)\Gamma(3q_u + 1)} \left[p_4^3 p_2^1 + p_4^1 p_2^3 + p_4^2 p_2^2 \right] \Bigg]$$

$$p_5^5 = a_6 p_4^4 + a_7 \left[p_1^4 p_3^0 + p_1^0 p_3^4 \right]$$

$$+ \frac{\Gamma(4q_v + 1)}{\Gamma(q_v + 1)\Gamma(3q_v + 1)} \left[p_1^3 p_3^1 + p_1^1 p_3^3 + p_1^2 p_3^2 \right] \Bigg]$$

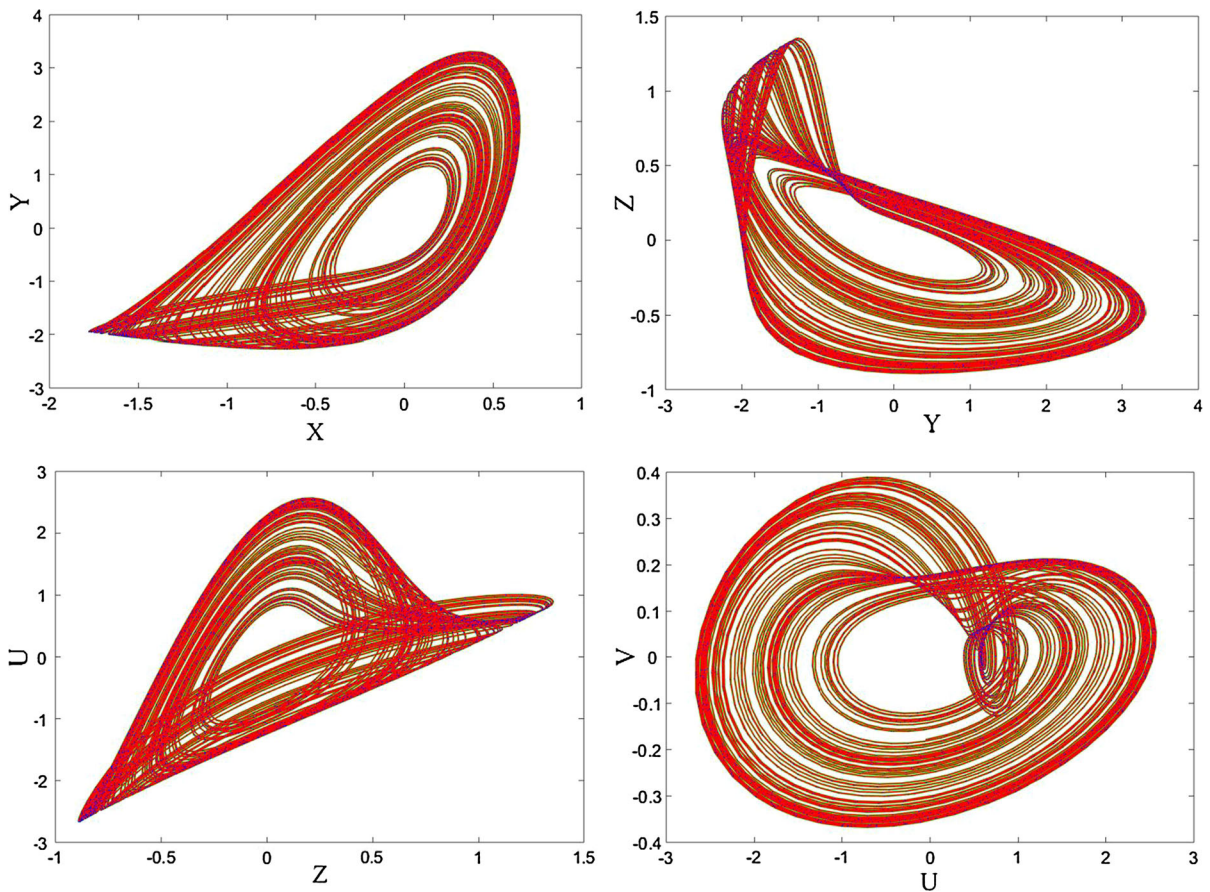$$+ a_8 p_3^4 + a_9 p_5^4 + a_0 \tag{32}$$

Fig. 13 2D phase portraits of the FPGA-implemented MCO system for $a \neq 0$. The initial conditions and parameter values are taken as in Sect. 2, and the order of the system is $q = 0.993$

The Adomian sixth polynomial is derived as,

$$p_1^6 = p_3^5$$
$$p_2^6 = p_4^5$$
$$p_3^6 = a_1 p_3^5 + a_2 \left[p_1^5 p_3^0 + p_1^0 p_3^5 + \frac{\Gamma(5q_z + 1)}{\Gamma(q_z + 1)\Gamma(4q_z + 1)} \right.$$
$$\left. \times \left[p_1^4 p_3^1 + p_1^1 p_3^4 + p_1^3 p_3^2 + p_1^2 p_3^3 \right] \right] + a_3 p_5^5$$
$$p_4^6 = a_4 p_5^5 + a_5 p_4^5 + a_5 \left[p_4^5 p_2^0 + p_4^0 p_2^5 \right.$$
$$+ \frac{\Gamma(5q_u + 1)}{\Gamma(q_u + 1)\Gamma(4q_u + 1)}$$
$$\left. \times \left[p_4^4 p_2^1 + p_4^1 p_2^4 + p_4^3 p_2^2 + p_4^2 p_2^3 \right] \right]$$
$$p_5^6 = a_6 p_4^5 + a_7 \left[p_1^5 p_3^0 + p_1^0 p_3^5 \right.$$
$$+ \frac{\Gamma(5q_v + 1)}{\Gamma(q_v + 1)\Gamma(4q_v + 1)}$$

$$\left[p_1^4 p_3^1 + p_1^1 p_3^4 + p_1^3 p_3^2 + p_1^2 p_3^3 \right] \right]$$
$$+ a_8 p_3^5 + a_9 p_5^5 + a_0 \tag{33}$$

where $h = t_{n+1} - t_n$ and $\Gamma(\bullet)$ is the gamma function. The fractional-order discretized system (27) is then implemented in FPGA, and the necessary Adomian polynomials are calculated using (28)–(33). For implementing in FPGA, the value of h is taken as $0.001s$ and the initial conditions are fed into the forward register with fractional order taken as $q = 0.995$ and $q = 0.993$ for MCO system with $a = 0$ and $a \neq 0$, respectively. Figure 9 shows the RTL schematics of the MCO system implemented in Kintex 7. Figures 10a and 11a show the power consumed by MCO system for order $a = 0$ and $a \neq 0$, respectively, and Figs. 10b and 11b show the power consumed for various fractional orders of $a = 0$ and $a \neq 0$, respectively, and it can be seen that maximum power is consumed when the MCO system

exhibits the largest Lyapunov exponent. Tables 1 and 2 show the resources consumed with the consumed clock frequencies, and Figs. 12 and 13 show the 2D phase portraits of the FPGA-implemented MCO system for $a = 0$ and $a \neq 0$, respectively.

5 Conclusion

Fractional-order models of memristor and memcapacitor are derived and used to design a memfractor chaotic oscillator. The oscillator shows self-excited and hidden flows depending on the value of the parameter a_0, thus showing a chameleon-like behavior. Bifurcation plots are derived and investigated. Adomian decomposition method is used to derive the discrete version of the proposed chaotic oscillator for implementing in FPGA.

References

1. Chua, L.O.: Memristor—the missing circuit element. IEEE Trans. Circuit Theory **18**(5), 507–519 (1971)
2. Strukov, D.B., Snider, G.S., Stewart, G.R., Williams, R.S.: The missing memristor found. Nature **453**, 80–83 (2008)
3. Buscarino, A., Fortuna, L.: A gallery of chaotic oscillators based on HP memristor. Int. J. Bifurc. Chaos **23**, 1–13 (2013)
4. Barboza, R., Chua, L.O.: The four-element Chuas circuit. Int. J. Bifurc. Chaos. **18**, 943–955 (2008)
5. Bao, B., Liu, Z., Xu, J.: Dynamical analysis of memristor chaotic oscillator. Acta Phys. Sin. **59**, 3785–3793 (2010)
6. Chua, L.O., Kang, S.M.: Memristive devices and systems. Proc. IEEE **64**, 209–223 (1976)
7. Muthuswamy, B., Kokate, P.P.: Memristor based chaotic circuits. IETE Tech. Rev. **26**, 417–429 (2009)
8. Kim, H., Sah, M.P., Yang, C., Cho, S., Chua, L.O.: Memristor emulator for memristor circuit applications. IEEE Trans. Circuits Syst. I Reg. Pap. **59**(10), 2422–2431 (2012)
9. Buscarino, A., Fortuna, L., Frasca, M., Valentina Gambuzza, L.: A chaotic circuit based on Hewlett–Packard memristor. Chaos **22**, 023136 (2012)
10. Hong, Q.-H., Li, Z.-J., Zeng, J.-F., et al.: Design and simulation of a memristor chaotic circuit based on current feedback op amp. Acta Phys. Sin. **63**(18), 180502 (2014)
11. Wang, G., Cui, M., Cai, B., Wang, X., Hu, T.: A chaotic oscillator based on HP memristor model. Math. Probl. Eng. **2015**, 1–12 (2015)
12. Wang, Z., Mina, F., Wang, E.: A new hyperchaotic circuit with two memristors and its application in image encryption. AIP Adv. **6**, 095316 (2016)
13. Muthuswamy, B.: Implementing memristor based chaotic circuits. Int. J. Bifurc. Chaos **20**, 1335 (2010)
14. Corinto, F., Krulikovskyi, O.V., Haliuk, S.D.: Memristor-based chaotic circuit for pseudo-random sequence generators. In: 18th Mediterranean Electrotechnical Conference (MELECON). Lemesos, pp. 1–3 (2016)
15. Yang, C., Hu, Q., Yu, Y., Zhang, R., Yao, Y., Cai, J.: Memristor-based chaotic circuit for text/image encryption and decryption. In: 8th International Symposium on Computational Intelligence and Design (ISCID). Hangzhou, pp. 447–450 (2015)
16. Wang, G., Jiang, S., Wang, X., Shen, Y., Yuan, F.: A novel memcapacitor model and its application for generating chaos. Math. Probl. Eng. **2016**, 1–15 (2016)
17. Rajagopal, K., Laarem, G., Karthikeyan, A., Srinivasan, A., Adam, G.: Fractional order memristor no equilibrium chaotic system with its adaptive sliding mode synchronization and genetically optimized fractional order PID synchronization. Complexity **2017**, 1–19 (2017)
18. Rajagopal, K., Karthikeyan, A., Srinivasan, A.: FPGA implementation of novel fractional order chaotic system with two equilibriums and no equilibrium and its adaptive sliding mode synchronization. Nonlinear Dyn. **87**(4), 2281–2304 (2017)
19. Baleanu, D., Diethelm, K., Scalas, E., Trujillo, J.J.: Fractional Calculus: Models and Numerical Methods. World Scientific, Singapore (2014)
20. Zhou, Y.: Basic Theory of Fractional Differential Equations. World Scientific, Singapore (2014)
21. Diethelm, K.: The Analysis of Fractional Differential Equations. Springer, Berlin (2010)
22. Aghababa, M.P.: Robust finite-time stabilization of fractional-order chaotic systems based on fractional Lyapunov stability theory. J. Comput. Nonlinear Dyn. **7**, 21–31 (2012)
23. Boroujeni, E.A., Momeni, H.R.: Nonfragile nonlinear fractional order observer design for a class of nonlinear fractional order systems. Signal Process. **92**, 2365–2370 (2012)
24. Zhang, R., Gong, J.: Synchronization of the fractional-order chaotic system via adaptive observer. Syst. Sci. Control Eng. **2**(1), 751–754 (2014)
25. Li, R.H., Chen, W.S.: Fractional order systems without equilibria. Chin. Phys. B **22**, 040503 (2013)
26. Cafagna, D., Grassi, G.: Fractional-order systems without equilibria: the first example of hyperchaos and its application to synchronization. Chin. Phys. B **24**(8), 080502 (2015)
27. Danca, M.-F., Tang, W.K.S., Chen, G.: Suppressing chaos in a simplest autonomous memristor-based circuit of fractional order by periodic impulses. Chaos Solitons Fractals **84**, 31–40 (2015)
28. Petras, I.: Method for simulation of the fractional order chaotic systems. Acta Montan. Slov. **11**(4), 273–277 (2006)
29. Trzaska Zdzislaw, W.: Matlab solutions of chaotic fractional order circuits. Intech Open (2013). http://www.intechopen.com/download/pdf/21404. Accessed 27 Apr 2017
30. Pezeshki, C.: Bispectral analysis of systems possessing chaotic motions. J. Sound Vib. **137**(3), 357–368 (1990)
31. Tlelo-Cuautle, E., Pano-Azucena, A.D., Rangel-Magdaleno, J.J.: Generating a 50-scroll chaotic attractor at 66 MHz by using FPGAs. Nonlinear Dyn. **85**(4), 2143–2157 (2016)
32. Wang, Q., Yu, S., Li, C.: Theoretical design and FPGA-based implementation of higher-dimensional digital chaotic systems. IEEE Trans. Circuits Syst. I Reg. Pap. **63**(3), 401–412 (2016)

33. Dong, E., Liang, Z., Du, S.: Topological horseshoe analysis on a four-wing chaotic attractor and its FPGA implementation. Nonlinear Dyn. **83**(1–2), 623–630 (2016)

34. Tlelo-Cuautle, E., Carbajal-Gomez, V.H., Obeso-Rodelo, P.J.: FPGA realization of a chaotic communication system applied to image processing. Nonlinear Dyn. **82**(4), 1879–1892 (2015)

35. Rashtchi, V., Nourazar, M.: FPGA implementation of a real-time weak signal detector using a duffing oscillator. Circ. Syst. Signal Process. **34**(10), 3101–3119 (2015)

36. Tlelo-Cuautle, E., Rangel-Magdaleno, J.J., Pano-Azucena, D.: FPGA realization of multi-scroll chaotic oscillators. Commun. Nonlinear Sci. **27**(1–3), 66–80 (2015)

37. Ya-Ming, X., Li-Dan, W., Shu-Kai, D.: A memristor-based chaotic system and its field programmable gate array implementation. Acta Phys. Sin. 65(12), 120503 (2016)

38. Leenaerts, D.M.W.: Higher order spectral analysis to detect power-frequency mechanism in a driven Chua's circuit. Int. J. Bifurc. Chaos **7**(6), 1431–1440 (1997)

39. Pradhan, C., Jena, S.K., Nadar, S.R., Pradhan, N.: Higher-order spectrum in understanding nonlinearity in EEG rhythms. Comput. Math. Methods Med. **2012**, 1–8 (2012)

40. Karthikeyan, R., Laarem, G., Sundarapandian, V., Anitha, K., Ashokkumar, S.: Dynamical analysis and FPGA implementation of a novel hyperchaotic system and its synchronization using adaptive sliding mode control and genetically optimized PID control. Math. Probl. Eng. **2017**, 1–14 (2017)

41. Karthikeyan, R., Anitha, K., Prakash, D.: Hyperchaotic chameleon: fractional order FPGA implementation. Complexity **2017**, 1–16 (2017)

42. Charef, A., Sun, H.H., Tsao, Y.Y.: Fractal system as represented by singularity function. IEEE Trans. Autom. Control **37**, 1465–1470 (1992)

43. Adomian, G.A.: Review of the decomposition method and some recent results for nonlinear equations. Math. Comput. Model. **13**, 17–43 (1990)

44. Sun, H.H., Abdelwahab, A.A., Onaral, B.: Linear approximation of transfer function with a pole of fractional power. IEEE Trans. Autom. Control **29**, 441–444 (1984)

45. Tavazoei, M.S., Haeri, M.: Unreliability of frequency-domain approximation in recognizing chaos in fractional-order systems. IET Signal Process. **1**, 171–181 (2007)

46. He, S.B., Sun, K.H., Wang, H.H.: Solving of fractional-order chaotic system based on Adomian decomposition algorithm and its complexity analyses. Acta Phys. Sin. **63**, 030502 (2014)

47. Caponetto, R., Fazzino, S.: An application of Adomian decomposition for analysis of fractional-order chaotic systems. Int. J. Bifurc. Chaos **23**, 1350050 (2013)

48. He, S., Sun, K., Wang, H.: Complexity analysis and DSP implementation of the fractional-order Lorenz hyperchaotic system. Entropy **17**, 8299–8311 (2015)

49. Wang, G., Shi, C., Wang, X., Yuan, F.: Coexisting oscillation and extreme multistability for a memcapacitor-based circuit. Math. Probl. Eng. **2017**, 1–13 (2017)

50. Wang, G., Jin, P., Wang, X., Shen, Y., Yuan, F., Wang, X.: A flux controlled model of meminductor and its application in chaotic oscillator. Chin. Phys. B **25**(9), 090502 (2016)

51. Pershin, Y.V., Di Ventra, M.: Emulation of floating memcapacitors and meminductors using current conveyors. Electron. Lett. **47**(4), 243–244 (2011)

52. Yu, D.S., Liang, Y., Chen, H., Iu, H.H.C.: Design of a practical memcapacitor emulator without grounded restriction. IEEE Trans. Circuits Syst. II Exp. Br. **60**(4), 207–211 (2013)

53. Fitch, A.L., Iu, H.H.C., Yu, D,: Chaos in a memcapacitor based circuit. In: Proceedings of the IEEE International Symposium on Circuits and Systems (ISCAS '14). IEEE, Sydney, Australia, pp. 482–485 (2014)

54. Fouda, M.E., Radwan, A.G.: Charge controlled memristor-less memcapacitor emulator. Electron. Lett. **48**(23), 1454–1455 (2012)

55. Wang, G.-Y., Cai, B.-Z., Jin, P.-P., Hu, T.-L.: Memcapacitor model and its application in a chaotic oscillator. Chin. Phys. B. **25**(1), 010503 (2015)

56. Yuan, F., Wang, G., Shen, Y., Wang, X.: Coexisting attractors in a memcapacitor-based chaotic oscillator. Nonlinear Dyn. **86**(1), 37–50 (2016)

57. Li, C., Gong, Z., Qian, D.: On the bound of the Lyapunov exponents for the fractional differential systems. Chaos **20**, 013127 (2010)

58. Wolf, A., Swift, J.B., Swinney, H.L.: Determining Lyapunov exponents from a time series. Phys. D Nonlinear Phenom. **16**, 285–317 (1985)

59. Ellner, S., Gallant, A.R., McCaffrey, D.: Convergence rates and data requirements for Jacobian-based estimates of Lyapunov exponents from data. Phys. Lett. A **153**, 357–363 (1991)

60. Maus, A., Sprott, J.C.: Evaluating Lyapunov exponent spectra with neural networks. Chaos Solitons Fractals **51**, 13–21 (2013)

61. Oldham, B., Spanier, J.: The Fractional Calculus: Theory and Applications of Differentiation and Integration to Arbitrary Order. Academic, New York (1974)

62. Podlubny, I.: Fractional Differential Equations: An Introduction to Fractional Derivatives, Fractional Differential Equations, to Methods of Their Solution and Some of Their Applications. Academic, San Diego (1998)

63. Krishna, B.T.: Studies on fractional order differentiators and integrators: a survey. Signal Process. **91**(3), 386426 (2011)

64. Pu, Y.-F., Yuan, X.: Fracmemristor: fractional-order memristor. IEEE Access **4**, 1872–1888 (2016)

65. Fouda, M.E., Radwan, A.G.: On the fractional-order memristor model. J. Frac. Calc. Appl. **4**(1), 1–7 (2013)

66. Abdelouahab, S., Lozi, R., Chua, L.: Memfractance: a mathematical paradigm for circuit elements with memory. Int. J. Bifurc. Chaos. **24**(9), 1430023 (2014)

67. Radwan, G., Moaddy, K., Hashim, I.: Amplitude modulation and synchronization of fractional-order memristor-based Chua's circuit. Abstr. Appl. Anal. **2013**, 1–10 (2013)

68. Miller, K.S., Ross, B.: An Introduction to Fractional Calculus and Fractional Differential Equations. Wiley, New York (1993)

69. Abdelouahab, M.-S., Lozi, R., Chua, L.: Memfractance: a mathematical paradigm for circuit elements with memory. Int. J. Bifurc. Chaos. **24**(9), 1430023–29 (2014)

70. Danca, M.-F.: Lyapunov exponents of a class of piecewise continuous systems of fractional order. Nonlinear Dyn. **81**, 227 (2015)

71. Jafari, M.A., Mliki, E., Akgul, A.: Chameleon: the most hidden chaotic flow. Nonlinear Dyn. **88**(3), 2303–2317 (2017)

72. Kuznetsov, A.P., Kuznetsov, S.P., Mosekilde, E., Stankevich, N.V.: Co-existing hidden attractors in a radio physical oscillator system. J. Phys. A Math. Theor. **48**, 125101 (2015)

73. Bragin, V.O., Vagaitsev, V.I., Kuznetsov, N.V., Leonov, G.A.: Algorithms for finding hidden oscillations in nonlinear systems. The Aizerman and Kalman conjectures and Chua's circuits. J. Comput. Sci. Int. **50**, 511–543 (2011)

74. Leonov, G.A., Kuznetsov, N.V.: Hidden attractors in dynamical systems. From hidden oscillations in Hilbert–Kolmogorov, Aizerman, and Kalman problems to hidden chaotic attractors in Chua circuits. Int. J. Bifurc Chaos. **23**(1), 1330002 (2013)

75. Akgul, A., Calgan, H., Koyuncu, I., et al.: Chaos-based engineering applications with a 3D chaotic system without equilibrium points. Nonlinear Dyn. **84**, 481–495 (2016)

76. Leonov, G.A., Kuznetsov, N.V., Kiseleva, M.A., Solovyeva, E.P., Zaretskiy, A.M.: Hidden oscillations in mathematical model of drilling system actuated by induction motor with a wound rotor. Nonlinear Dyn. **77**(1–2), 277–288 (2014)

77. Leonov, G.A., Kuznetsov, N.V.: Analytical-numerical methods for investigation of hidden oscillations in nonlinear control systems. IFAC Proc. Vol. (IFAC-PapersOnline) **18**(1), 2494–2505 (2011)

78. Kuznetsov, N., Leonov, G.: Hidden attractors in dynamical systems: systems with no equilibria, multistability and coexisting attractors. IFAC Proc. Vol. (IFAC-PapersOnline) **19**, 5445–5454 (2014)

79. Leonov, G., Kuznetsov, N., Mokaev, T.: Homoclinic orbits, and self-excited and hidden attractors in a Lorenz-like system describing convective fluid motion. Eur. Phys. J. Spec. Top. **224**(8), 1421–1458 (2015)

80. Leonov, G.A., Kuznetsov, N.V., Vagaitsev, V.I.: Localization of hidden Chua's attractors. Phys. Lett. A **375**(23), 2230–2233 (2011)

81. Leonov, G.A., Kuznetsov, N.V., Vagaitsev, V.I.: Hidden attractor in smooth Chua systems. Physica D **241**(18), 1482–1486 (2012)

82. Leonov, G., Kuznetsov, N., Mokaev, T.: Homoclinic orbit and hidden attractor in the Lorenz-like system describing the fluid convection motion in the rotating cavity. Commun. Nonlinear Sci. Numer. Simul. **28**, 166–174 (2015)

83. Kuznetsov, N., Leonov, G.A., Mokaev, T.N.: Hidden attractor in the Rabinovich system (2015). arXiv:1504.04723v1

84. Jafari, S., Sprott, J.C., Golpayegani, S.M.R.H.: Elementary quadric chaotic flows with no equilibria. Phys. Lett. A **377**, 699–702 (2013)

85. Valli, D., et al.: Synchronization in coupled Ikeda delay systems. Eur. Phys. J. Spec. Top. **223**(8), 1465–1479 (2014)

86. Atteya, A.M., Madian, A.H.: A hybrid Chaos-AES encryption algorithm and its impelmention based on FPGA. In: IEEE 12th International on New Circuits and Systems Conference (NEWCAS), pp. 217–220 (2014)

87. Dadras, S., Momeni, H.R.: A novel three-dimensional autonomous chaotic system generating two, three and four-scroll attractors. Phys. Lett. A **373**(40), 3637–3642 (2009)

88. Dadras, S., Momeni, H.R., Qi, G., Wang, Z.: Four-wing hyperchaotic attractor generated from a new 4D system with one equilibrium and its fractional-order form. Nonlinear Dyn. **67**(2), 1161–1173 (2012)

89. Dadras, S., Dadras, S., Malek, H., Chen, Y.: A note on the Lyapunov stability of fractional order nonlinear systems. ASME Paper No. IDETC2017-68270 (2017)

90. Sharma, P.R., Shrimali, M.D., Prasad, A., Kuznetsov, N.V., Leonov, G.A.: Control of multistability in hidden attractors. Eur. Phys. J. Spec. Top. **224**, 1485 (2015)

91. Sharma, P.R., Shrimali, M.D., Prasad, A., Kuznetsov, N.V., Leonov, G.A.: Controlling dynamics of hidden attractors. Int. J. Bifurc. Chaos **25**, 1550061 (2015)

92. Karthikeyan, R., Akif, A., Sajad, J., Anitha, K., Ismail, K.: Chaotic chameleon: dynamic analyses, circuit implementation, FPGA design and fractional-order form with basic analyses. Chaos Solitons Fractals **103**, 476–487 (2017)

93. Li, C., Sprott, J.C., Hu, W., Xu, Y.: Infinite multistability in a self-reproducing chaotic system. Int. J. Bifurc. Chaos **27**(10), 1750160 (2017)

94. Li, C., Sprott, J.C.: How to bridge attractors and repellors. Int. J. Bifurc. Chaos **27**(10), 1750149 (2017)

95. Li, C., Wang, X., Chen, G.: Diagnosing multistability by offset boosting. Nonlinear Dyn. (2017). https://doi.org/10.1007/s11071-017-3729-1

96. Li, C., Sprott, J.C., Mei, Y.: An infinite 2-D lattice of strange attractors. Nonlinear Dyn. **89**, 2629–2639 (2017)

97. Li, C., Sprott, J.C., Akgul, A., Iu, H.H., Zhao, Y.: A new chaotic oscillator with free control. Chaos **27**, 083101 (2017)